Supplementary Information

Exploration of Biological Activities of Alkyne Arms containing Cu(II) and Ni(II) Complexes: Syntheses, Crystal Structures and DFT Calculations

Chithiraivel Balakrishnan[a], Satheesh Natarajan[b] and M.A. Neelakantan[a*]

[a]Chemistry Research Centre, National Engineering College, K. R. Nagar, Kovilpatti- 628503, Thoothukudi District, Tamil Nadu, India.

[b]Department of Pharmacy, School of Health Sciences, Kwazulu Natal University, Durban-4001, South Africa

*Corresponding Author

Tel: +91 94425 05839, Fax: +91 4632 232749

E-mail Address: drmaneelakantan@gmail.com; maneels@rediffmail.com

DNA binding experiments

The DNA binding test of Schiff bases and metal complexes with CT-DNA were performed at room temperature in double distilled water with Tris-HCl/NaCl buffer (50 mM Tris-HCl/1mM NaCl buffer, pH 7.2). The concentration of CT-DNA was measured by its extinction coefficient at 260 nm (6600 M^{-1} cm^{-1}) after 1:100 dilutions.[S1] Stock solutions were stored at 4°C and used not more than 4 days. The test compounds were dissolved in a mixed solvent of 5% acetonitrile and 95% Tris-HCl buffer solutions. Absorption titration experiments were done by keeping fixed concentration of compounds at 20 μM while gradually increasing CT-DNA concentration from 0 to 50 μM. During absorption titration equal amount of CT-DNA was added to both the test solution and reference solution to eliminate the absorbance of CT-DNA itself.

The competitive binding test of compounds with EB has been done by fluorescence spectroscopic technique in order to examine whether the complex can displace EB from its CT-DNA-EB complex. EB-bound CT-DNA solution was prepared using Tris-HCl/NaCl buffer (pH 7.2, 5 mM Tris-HCl, 50 mM NaCl). The experiments were carried out by adding a solution of compounds ([compound] = 1.0×10^{-3} M) into the EB DNA solution (30 μM EB and 20 μM CT-DNA). The change of fluorescence intensity was recorded with respect to different concentrations of the compounds (0 - 50 μM). The excitation and the emission wavelengths were 520 and 605 nm, respectively. Before the titrations, the test compounds-DNA solutions were incubated at room temperature for 5 min in order to full reaction.

Also, the time-resolved fluorescence lifetime measurements were carried out on the Horiba JobinYvon spectrofluorometer with 370 and 600 nm as excitation and emission wavelengths. The concentrations of samples were used as follows, [CT-DNA] = 40 μM; [EB] = 5 μM and [Complex] = 50, 100, 150, 200 and 250 μM. PBS (pH 7.2) was used to prepare the samples.

Viscosity studies

Viscosity measurements were carried out using an Ostwald-type viscometer maintained at 28 °C in a thermostatic water bath. The concentration of CT-DNA was kept constant (100 μM) and the concentration of metal complexes varied (10-100 μM). The flow time of samples solutions in phosphate buffer (pH 7.2) was measured in triplicate for each sample and an average flow time was calculated. The relative viscosity values were determined using the expression $\eta = (t - t_o)/t_o$, where t and t_o are the observed flow time of the DNA and buffer solution, respectively. The

relative viscosity values were presented as $(\eta/\eta_o)^{1/3}$ vs. [complex]/[DNA] binding ratio, where η is the viscosity of DNA in the presence of compound and η_o is the viscosity of DNA alone.

BSA protein binding studies

The protein binding studies of Schiff bases and their metal complexes were performed with fixed excitation wavelength corresponding to BSA at 280 nm and monitoring the emission at 337 nm. The excitation and emission slit widths and the scan rates were maintained constant for all the experiments. The BSA protein stock solution was prepared in 50 mM phosphate buffer (pH 7.2) and stored in the dark at 4°C for further use. The concentrated stock solution of the samples were prepared as mentioned for the DNA binding experiments, except that the phosphate buffer was used instead of a Tris-HCl buffer for all of the experiments. A solution of BSA (1.0×10^{-6} M) was titrated with different concentrations of samples (0 - 50 μM). Fluorescence spectra of the samples were recorded in the wavelength range of 290 - 450 nm upon excitation at 280 nm. Synchronous fluorescence spectra were also recorded with the same concentration of BSA and the complexes corresponding to the Δλ values (difference between the excitation and emission wavelengths of BSA), 15 and 60 nm.

DNA-cleavage experiment

DNA cleavage experiments were performed using supercoiled (SC) pUC19 DNA in 50 mM Tris-HCl/10 mM NaCl buffer. Stock solutions of complexes were prepared in acetonitrile and the pH was adjusted to 7 - 8 by addition of base. Reactions were carried out incubating DNA (5 μM) at 37 ± 0.2°C in the presence/absence of increasing amount of metal complexes. After incubation, the samples were immediately loaded on 0.8% agarose gel for electrophoresis in TBE buffer (50 mM Tris base, 25 mM boric acid, 2 mM EDTA) at 50 V for 2 hours. Finally the gel was photographed under UV light. When required, the incubation was performed in the same buffer but in the presence of hydroxyl radical scavengers (DMSO, KI, 0.1 mM), singlet oxygen quenchers (L-histidine, 0.25 μM), superoxide scavenger (superoxide dismutase enzyme SOD, 4 units) and chelating agent (EDTA, 5mM) under our experimental conditions.

Procedure for DNA ligation study

After incubation of DNA with increasing concentration of complexes for 1 h at 37 ± 0.2°C, the cleavage reactions were sanitized on a G-25 column. The plasmid was then incubated for 12 h at 10°C with T4 ligase (10 U/mL). The control experiments of the T4 ligase reactions were performed also on pUC19 DNA. The reaction products were resolved on a 1% agarose gel in

TBE buffer (50 mM Tris base, 25 mM boric acid, 2 mM EDTA) in the presence/absence of 1 μM ethidium bromide.

Cell culture

Cancer cell (HeLa) was obtained from the K-RITH, Durban, South Africa. The cells were cultured in RPMI 1640 medium containing 10% fetal bovine serum, 100 UmL^{-1} penicillin and 100 μg mL^{-1} streptomycin as antibiotics in 96-well culture plates at 37°C under a humidified atmosphere of 2% CO_2 in a CO_2 incubator. Cisplatin was purchased from Whitescience, South Africa. All the experiments were carried out using cells from passage 15 or less.

Evaluation of cytotoxicity and IC_{50}

Cytotoxicity effect of metal complexes [$Cu(L^1)$, $Ni(L^1)$, $Cu(L^2)$ and $Ni(L^2)$] was evaluated against HeLa cell using the micro-titration colorimetric method.[S2] The tetrazolium salt of 3-[4,5-dimethylthiazol-2-yl]-2,5diphenyl tetrazolium bromide (MTT) was used to find out cell viability in assays of cell proliferation and cytotoxicity. MTT powder (0.5 mg/mL) was dissolved in DPBS solution (stock solution of MTT (5 mg/mL)). The stock solution of MTT was filtered and sterilized through a 0.25 μM filter and stored at −20°C. MTT assay was transforming the yellow tetrazolium salt of MTT to purple formazan crystals by using metabolically active cells. HeLa cells were plated in 96-well microplates and three replica wells were used for controls. Then the cancerous cell was treated with complexes in acetonitrile for 24 h in a 2% CO_2 humidified atmosphere with cisplatin as control. After 24 h, the medium was removed and the formazan precipitate was dissolved using dimethylsulfoxide. The absorbance of the samples was measured at 570 nm with an ELISA multi-well plate reader. Each experiment was performed in triplicate. The relative viability of the treated cells compared to the control cells is expressed as % of cytoviability, using the following equation,

$$\% \text{ of viability} = (\text{OD value of sample treated cells} \times \text{OD value of untreated cells})/100$$

Annexin V-propidium iodide staining assay

Cell death by the metal complexes were evaluated by staining the cells with FITC (Flourescein isothiocyanate) tagged Annexin-V and Propidium Iodide (PI). HeLa cells were seeded in 6-well plate and incubated for 24 h. After 24 h, the medium was removed and a fresh culture of DMEM containing metal complexes (10 μmol L^{-1}) was added and incubated for 48 h at 35°C. Then the cells were harvested and washed with 50 mM PBS (pH 7.2). Cell pellet was then re-suspended in 100 μL of Annexin binding buffer and 5 μL of AnnexinV-FITC was added in the dark at room temperature. The samples were taken for flow cytometry analysis by using a BD Biosciences

FACSTM flow cytometry after 15 min of incubation with the propidium iodide (PI). Data analysis was carried out using FlowJo 7.6 software.

Comet assay

DNA damage was measured by comet assay as illustrated in the literature.[S3] Cells at a density of 5.0×10^4 mL^{-1} were plated in 6-well plates and treated with the metal complexes (1 μmol L^{-1}) at IC_{50} dose and cells were harvested by a trypsinization process at 24 h. After 24 hrs, the cell suspension were mixed with 1% low melting (37°C) agarose and spread on the pre-coated wells using normal melting agarose-coated (1% in PBS at 65°C) slides. The slides were immersed in lysis solution (pH 10, 0.25 M NaCl, 10 mM disodium EDTA (Na_2EDTA), 1 mM Tris base, 1% Triton-X 100 and 10% DMSO) at 4°C for 24 h. Then the lysis solution was poured off and the slides were submerged in a freshly prepared alkaline solution (pH > 13, 30 mM NaOH and 1 mM Na_2EDTA) in a horizontal gel electrophoresis tank at 4°C for 30 min. Consequently, electrophoresis was done at 25 V at 4 °C for 15 min. After electrophoresis, the slides were removed, washed three times with PBS (pH 7.2) and dried in air. Finally, the slides were stained with 20 μL of EtBr (50 μg mL^{-1}) in PBS (pH 7.2) solution. The photographs were taken using a Nikon Eclipse Ti fluorescence microscope equipped with an excitation filter of 520 - 560 nm and a barrier filter of 590 nm. The images were used to assess the degree of DNA fragmentation representing a fraction of the total DNA in the tail.[S4]

Catalytic oxidation of 3,5-DTBC

The catecholase activity of the metal complexes (10^{-4} M) were evaluated by the oxidation of 3,5-di-tert-butylcatechol (3,5-DTBC, 100 equiv) in acetonitrile solution under aerobic conditions at room temperature. UV-Vis absorbance of the resultant reaction mixture was plotted with respect to wavelength at a regular time interval of 5 min in the wavelength range 280 - 500 nm. The rate dependence on substrate (DTBC) concentration was determined by keeping the catalyst concentration constant (10^{-4} M) and varying the substrate equivalents at 20, 40, 60, 80 and 100, respectively. The reactions were monitored spectrophotometrically by measuring the intensity of the absorbance of the quinone band at 400 nm as a function of time.

Detection of hydrogen peroxide in the catalytic reactions

The hydrogen peroxide (H_2O_2) was formed during the catalytic reaction was detected by spectrophotometrically. Reaction mixtures were prepared as in the kinetic experiments. After 1 h of reaction, the solution was acidified with H_2SO_4 until a pH of 2 was reached. In order to reduce the further oxidation, an equal volume of water was added and the formed quinone was extracted

three times with CH_2Cl_2. To the aqueous layer, 1 mL of 10% solution of KI and three drops of 3% solution of ammonium molybdate was added. In the presence of hydrogen peroxide I^- is oxidized to I_2, [$H_2O_2 + 2I^- + 2H^+ \rightarrow 2H_2O + I_2$], with an excess of iodide ions, the tri-iodide ion is formed according to the reaction $I_{2\,(aq)} + I^- \rightarrow I_3^-$. The formation of I_3^- could be monitored by spectrophotometrically (λ_{max} = 353 nm; ε = 26000 M^{-1} cm^{-1}) due to development of the characteristic I_3^- band, upon the reaction with I^-. (Fig. S37).

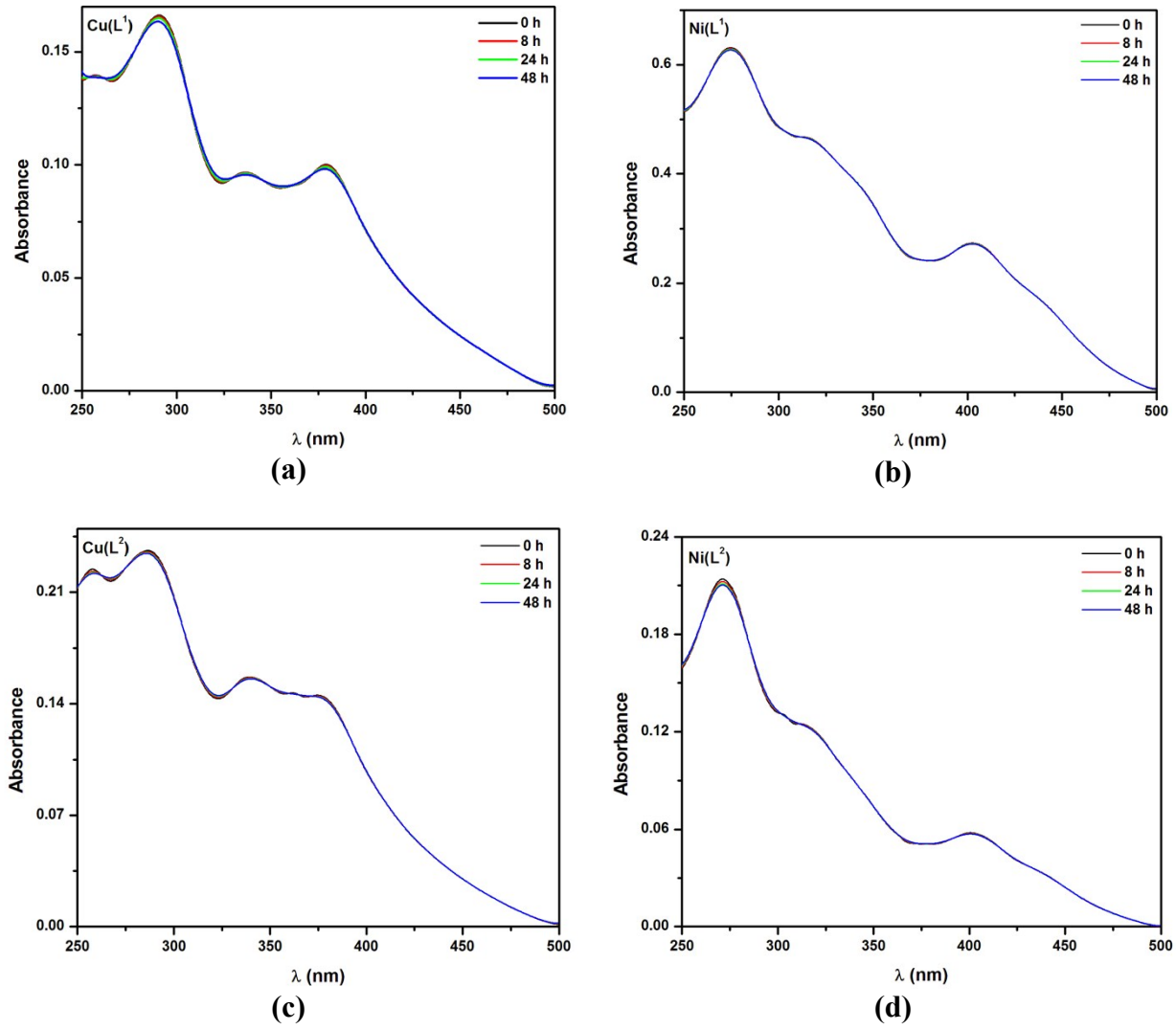

Fig. S1 Stability of the complexes, **(a)** Cu(L^1); **(b)** Ni(L^1); **(c)** Cu(L^2) and **(d)** Ni(L^2) measured by absorption spectroscopy in Tris-HCl buffer.

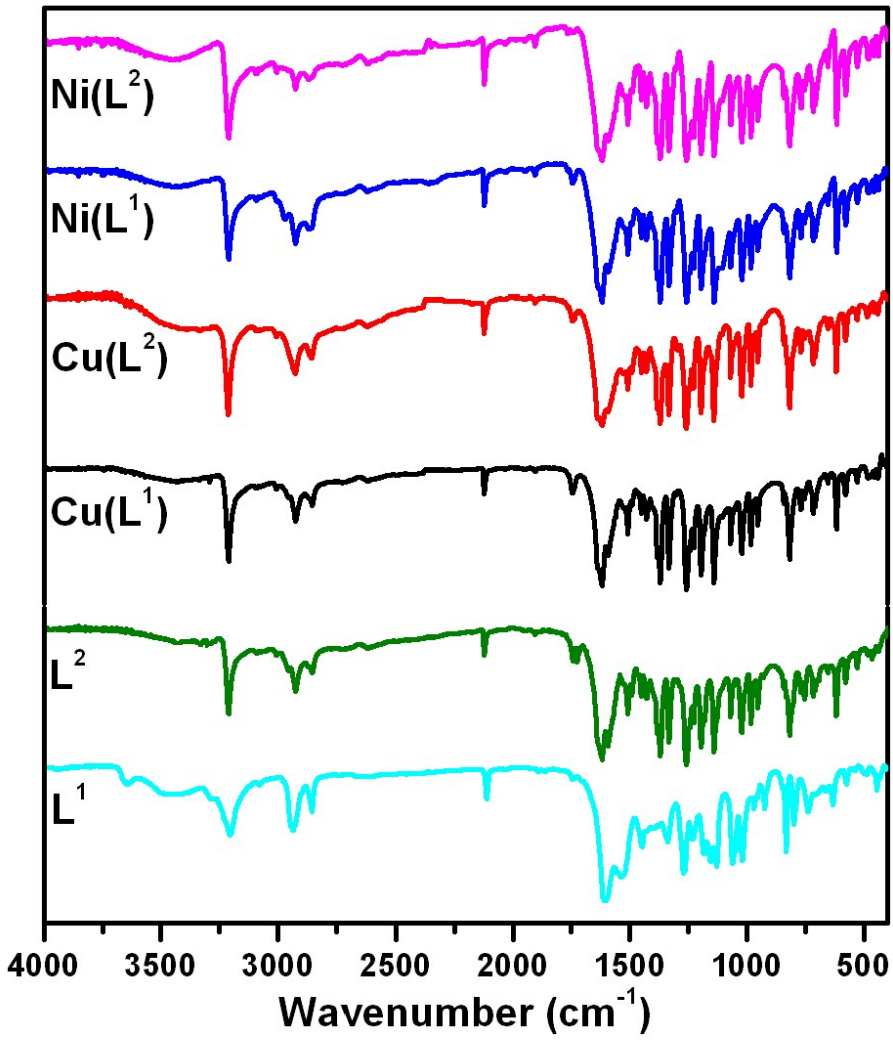

Fig. S2 FT-IR spectra of Schiff bases and their metal complexes.

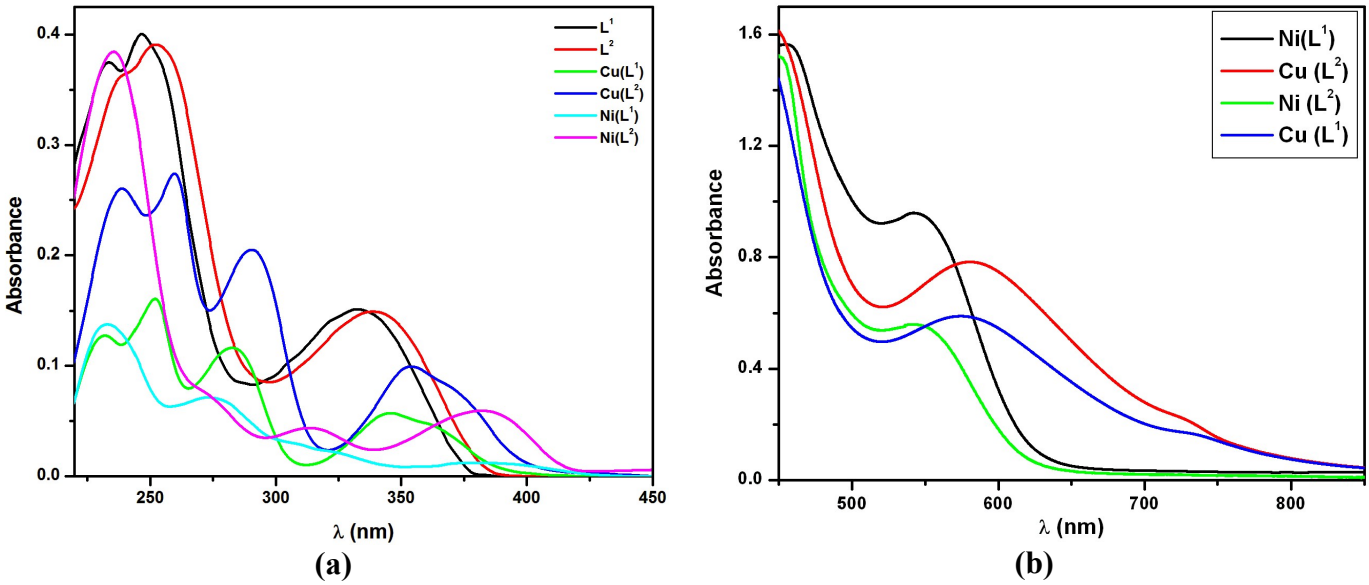

Fig. S3 Electronic spectra of, **(a)** ligands and their metal complexes (200 - 500 nm); **(b)** complexes (400 - 900 nm) in acetonitrile medium.

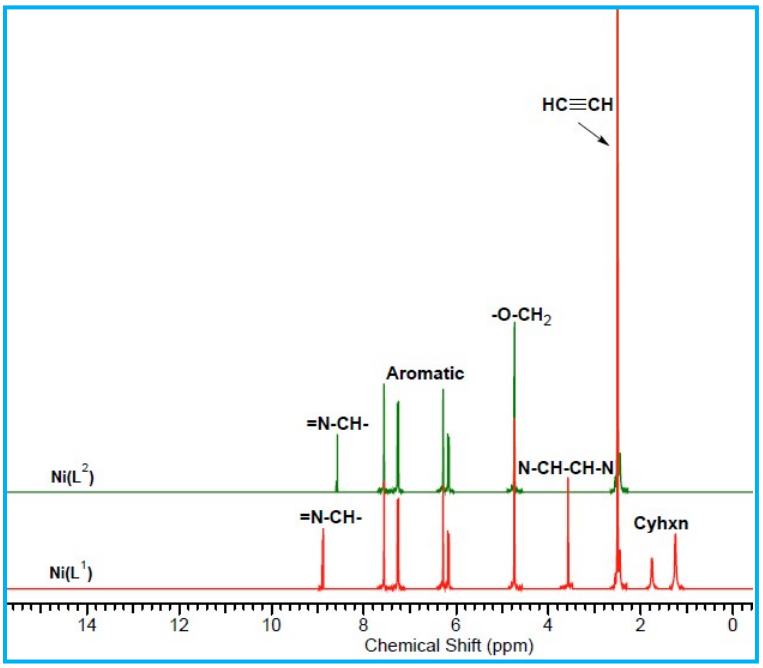

Fig. S4 ^{1}H NMR spectra of Ni(L^{1}), Ni(L^{2}) complexes.

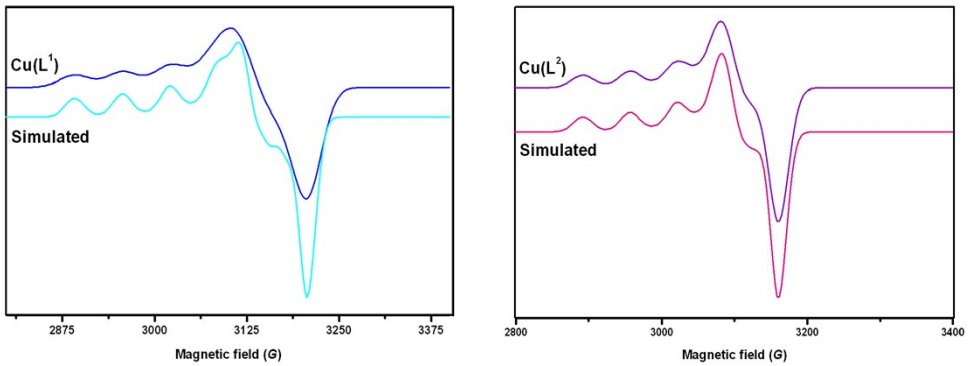

(a) **(b)**

Fig. S5 EPR spectra of (a) Cu(L^1) and (b) Cu(L^2) complexes at 77 K.

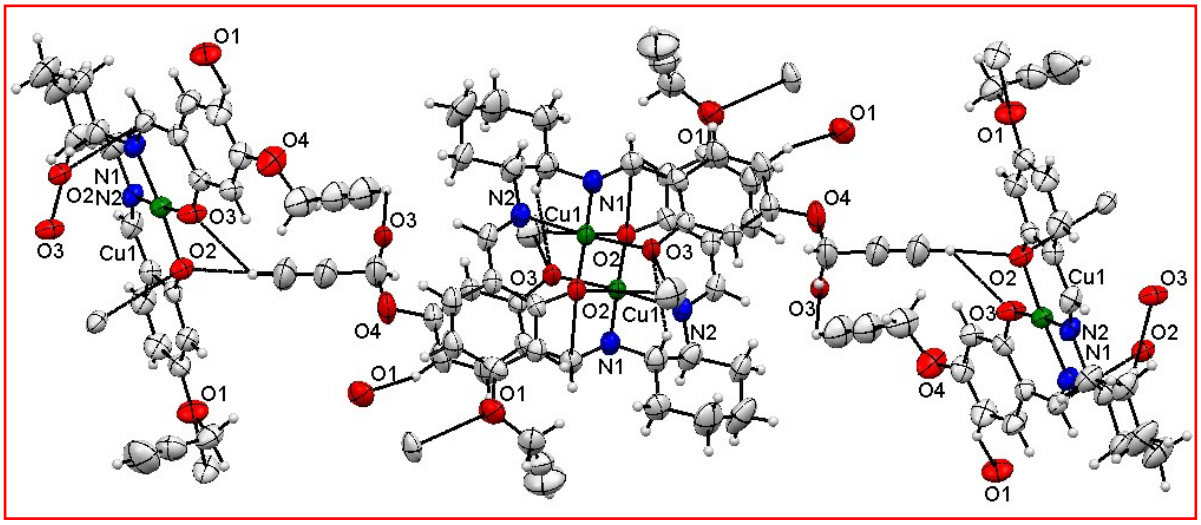

(a)

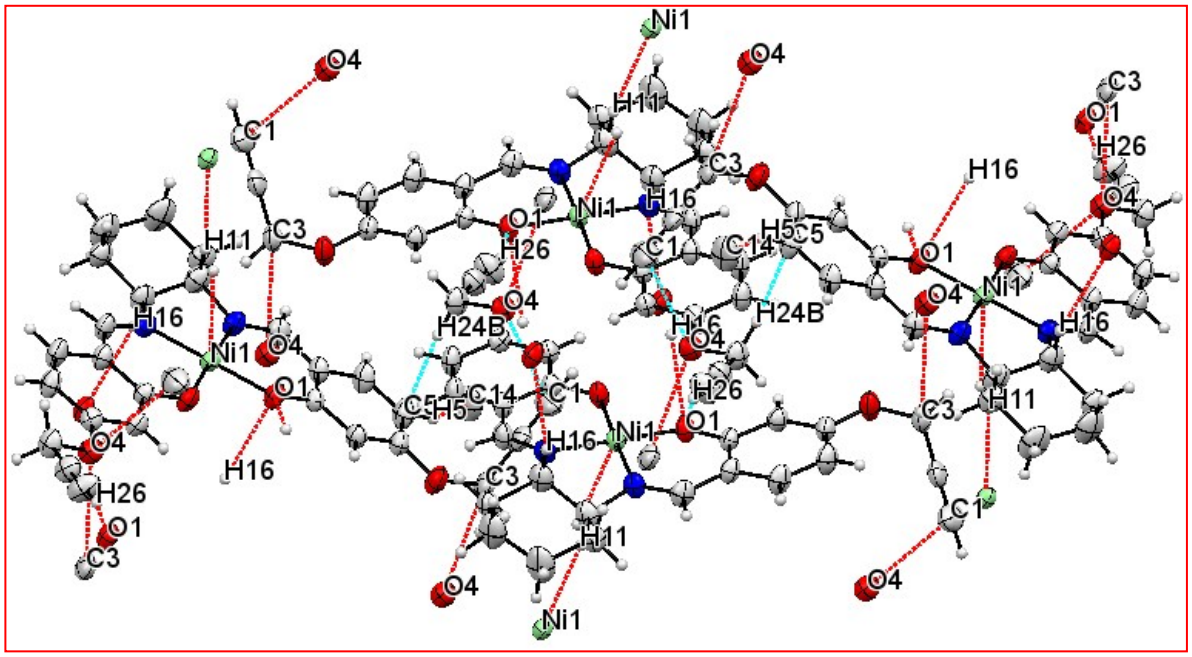

(b)

Fig. S6 Packing diagram showing the formation of 2D network of, (a) Cu(L^1) and (b) Ni(L^1) along the *a*-axis.

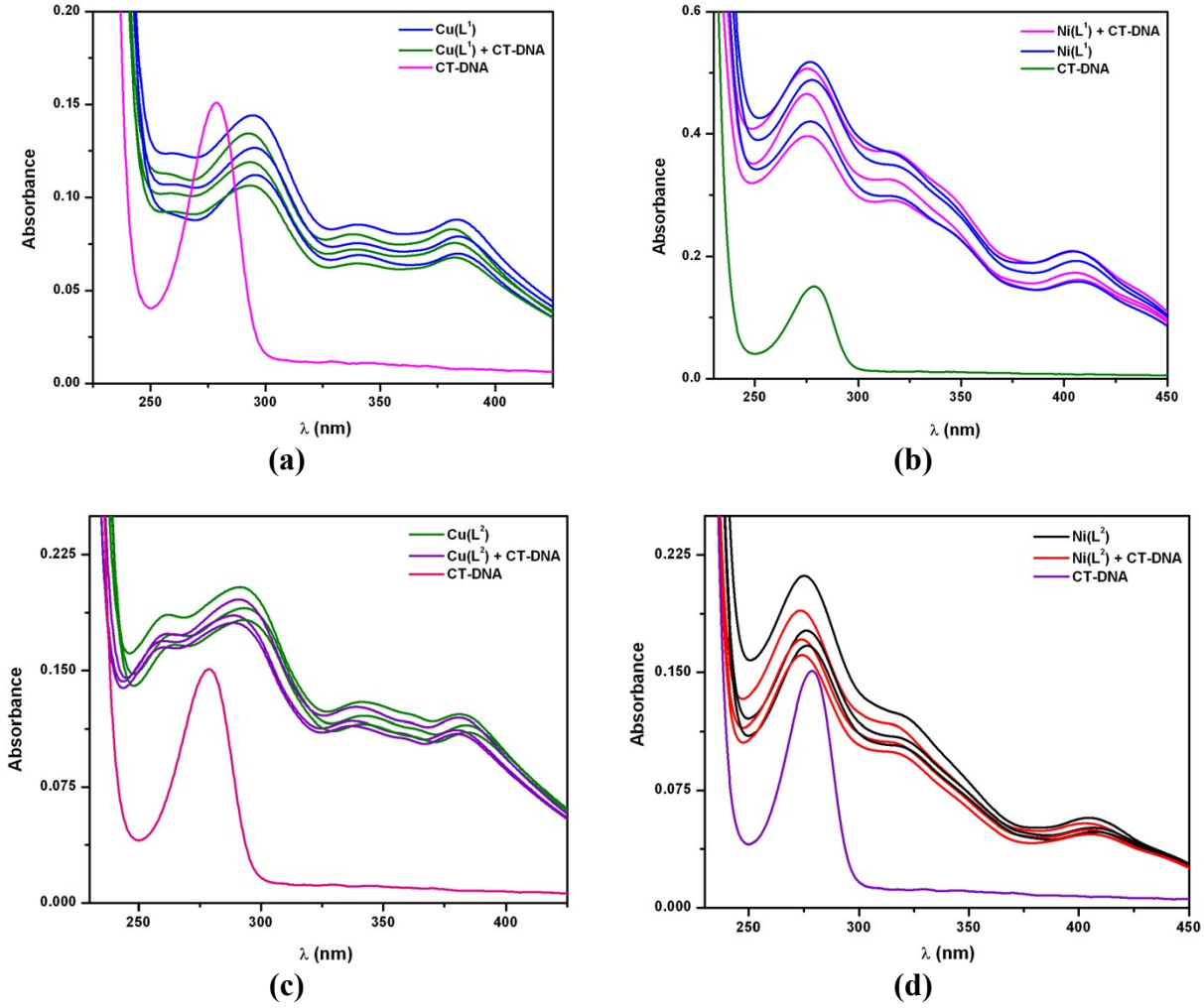

Fig. S7 Changes in electronic absorption spectra of **(a)** $Cu(L^1)$; **(b)** $Cu(L^2)$; **(c)** $Ni(L^1)$ and **(d)** $Ni(L^2)$ (5, 10 and 15 μM) after interactions with CT-DNA (100 μM) in Tris-HCl buffer.

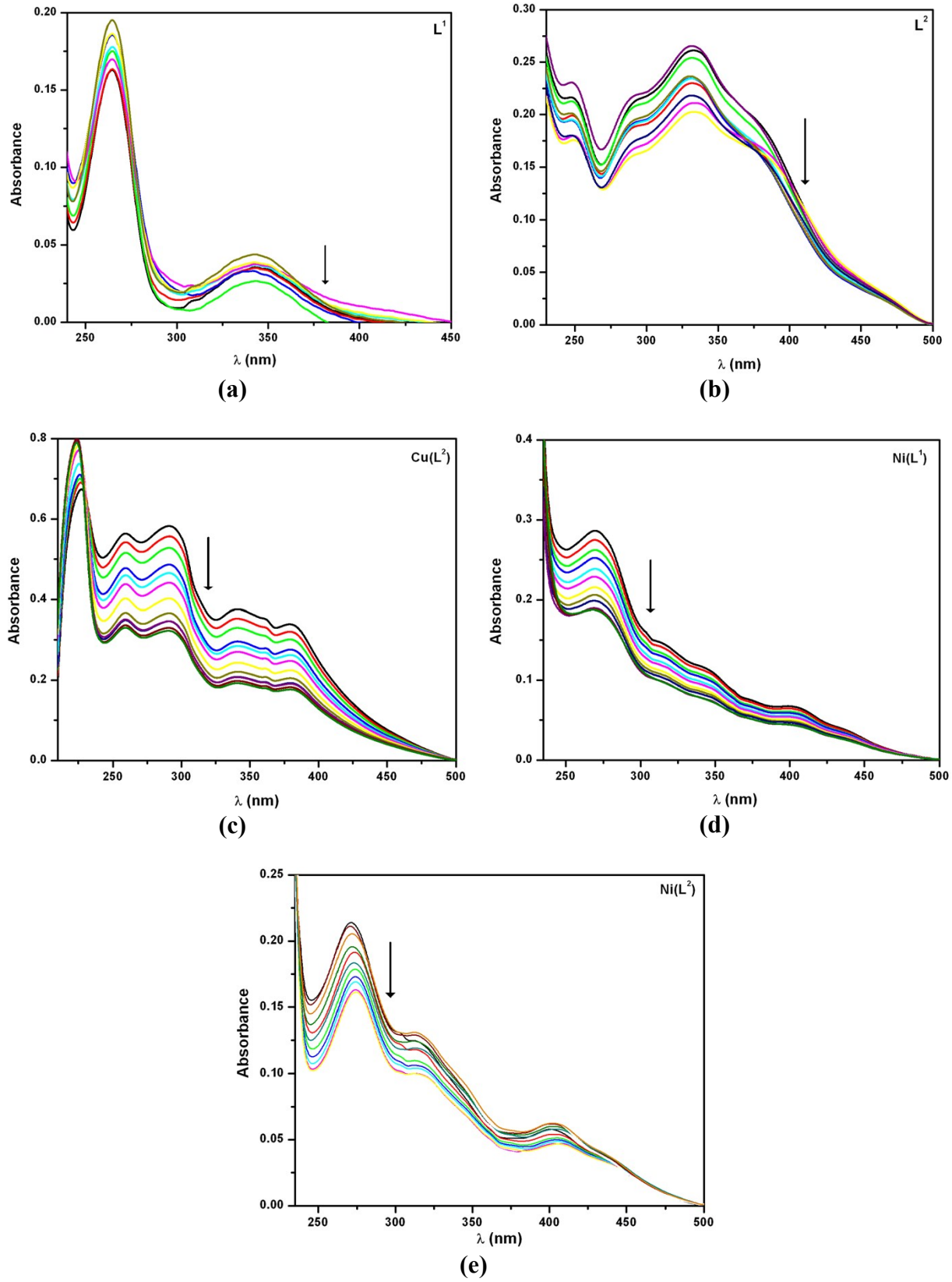

Fig. S8 Electronic absorption spectra of Schiff bases and their metal complexes, (a) L^1; (b) L^2; (c) $Cu(L^2)$; (d) $Ni(L^1)$ and (e) $Ni(L^2)$ in Tris-HCl buffer upon addition of CT-DNA (Arrow indicates that the absorption intensities decrease upon increasing DNA concentration).

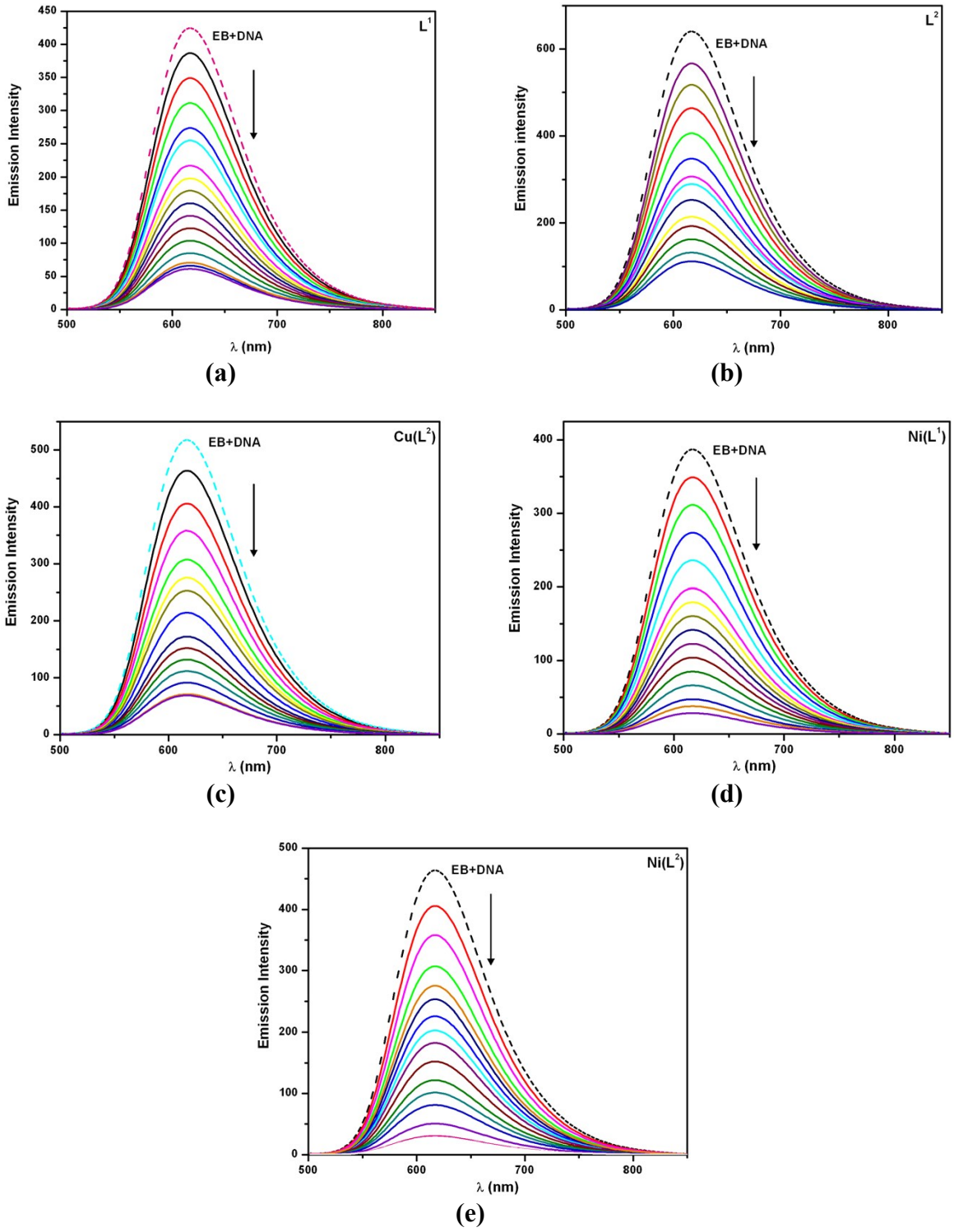

Fig. S9 Fluorescence quenching curves of EB bound to DNA in the presence of Schiff bases and their complexes, (a) L^1; (b) L^2; (c) $Cu(L^2)$; (d) $Ni(L^1)$ and (e) $Ni(L^2)$. (Arrow indicates that the absorption intensities decrease upon increasing DNA concentration).

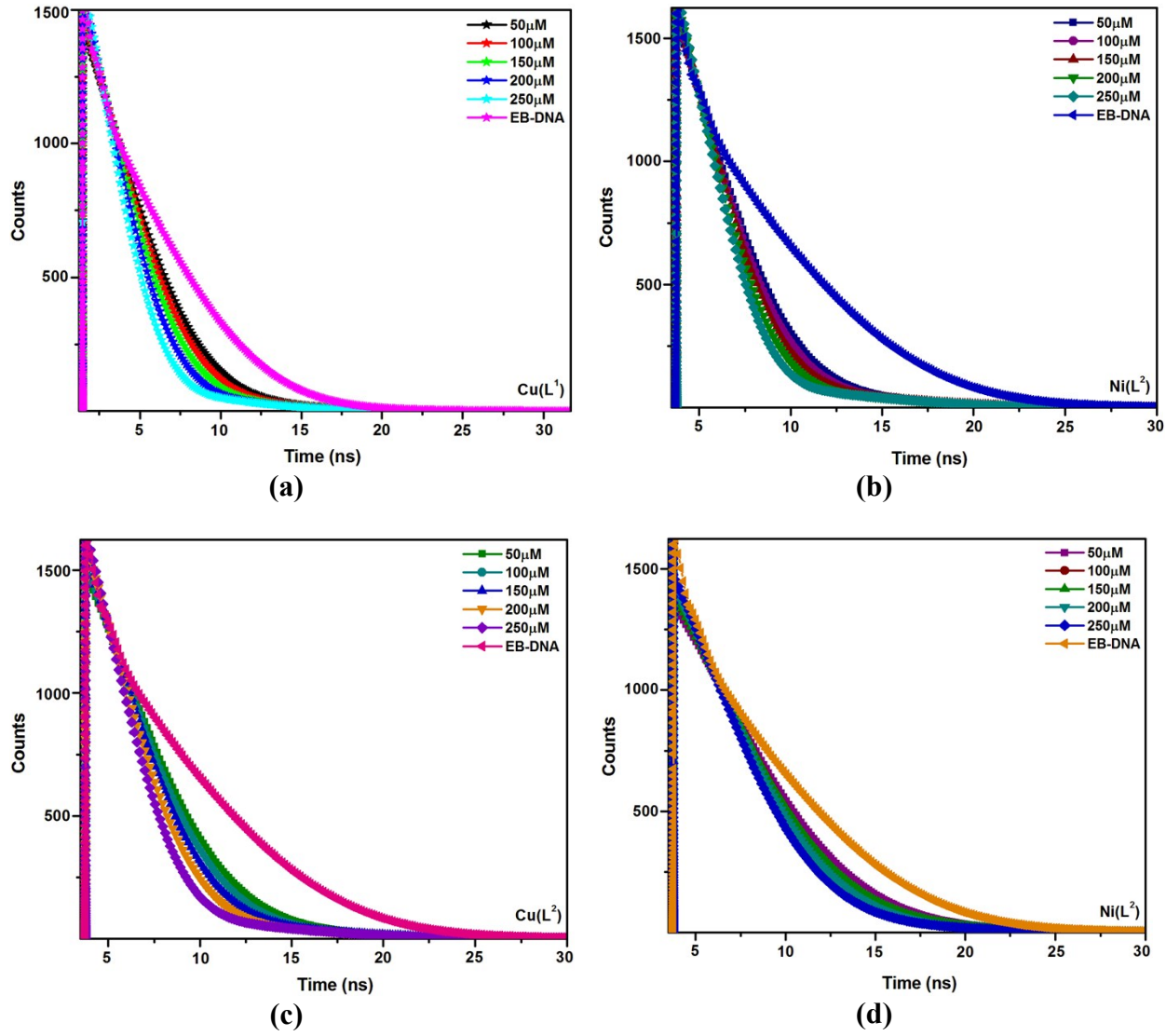

Fig. S10 Time-resolved fluorescence lifetime of EB-DNA complex and various concentrations of metal complexes with EB-DNA, (a) Cu(L^1); (b) Ni(L^1); (c) Cu(L^2) and (d) Ni(L^2) in PBS buffer (pH 7.2).

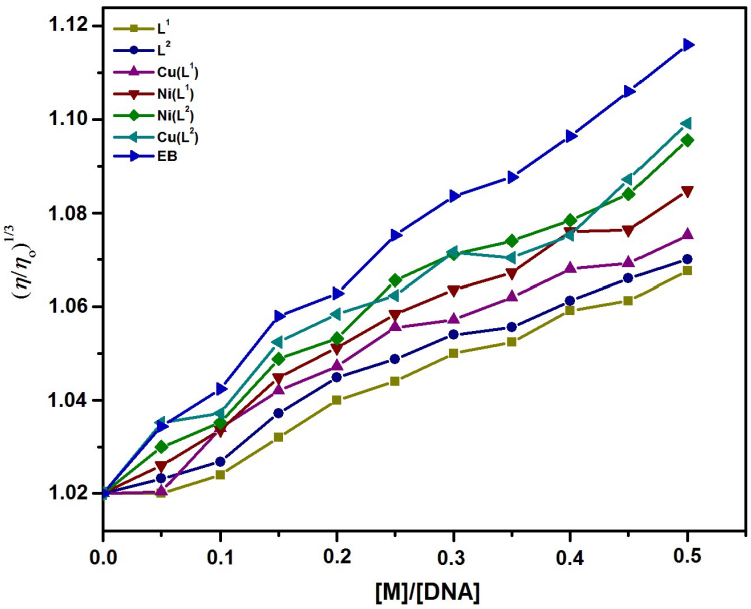

Fig. S11 Effects of increasing concentrations of the complexes (1-4) on the relative viscosities of the DNA in phosphate buffer.

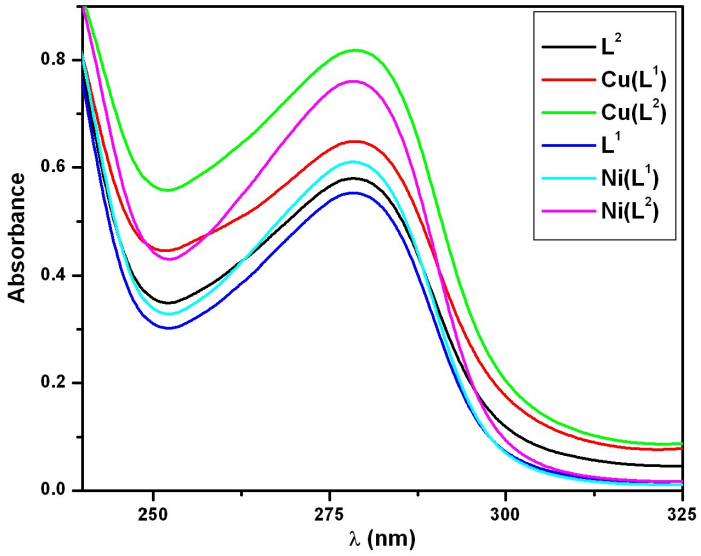

Fig. S12 The absorption spectra of BSA with Schiff bases and their metal complexes in Tris-HCl buffer.

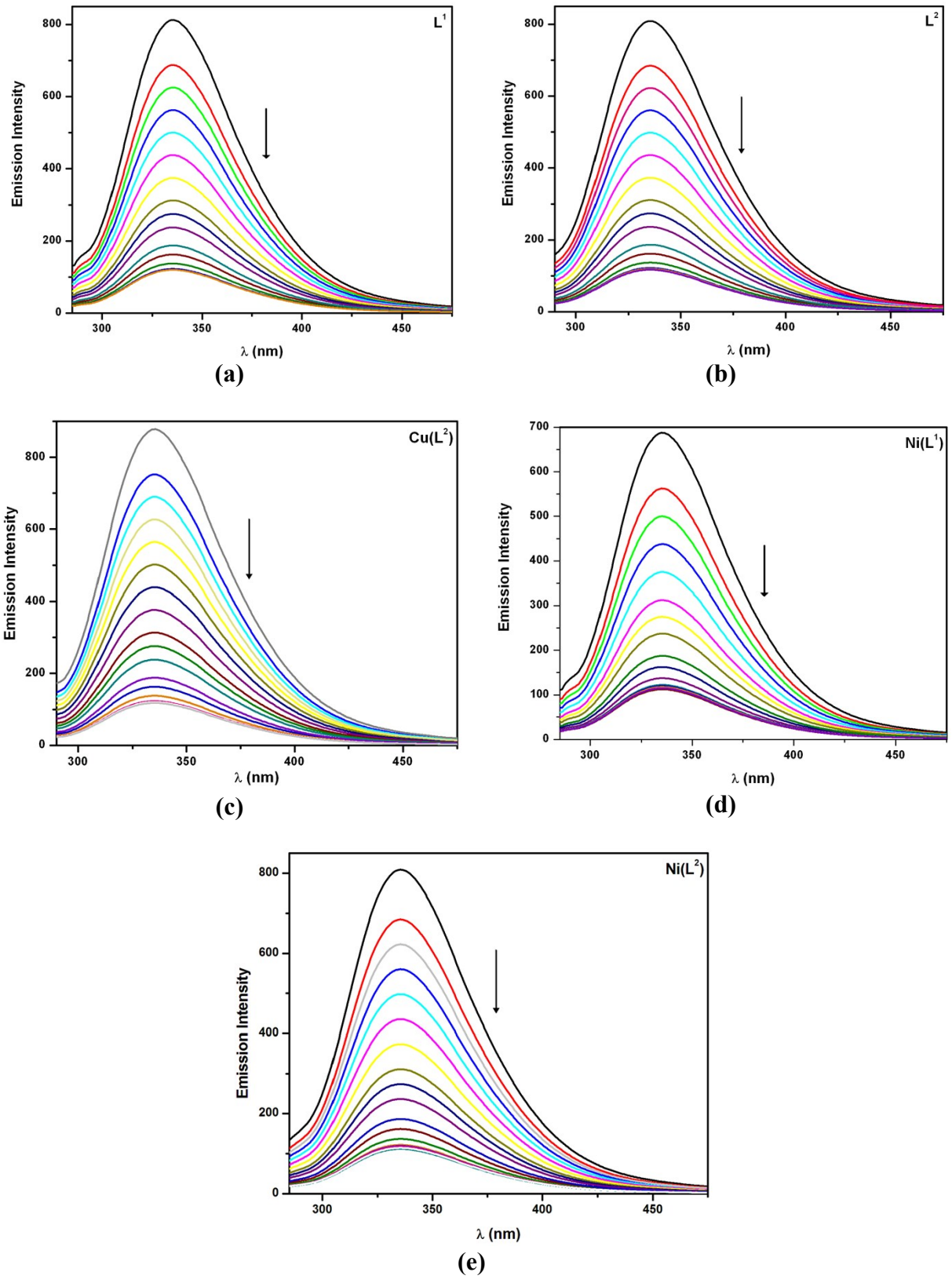

Fig. S13 Fluorescence quenching spectra of BSA in the presence of increasing amounts of the ligands and their metal complexes, (a) L^1; (b) L^2; (c) $Cu(L^2)$; (d) $Ni(L^1)$ and (e) $Ni(L^2)$. [BSA] = 1 μM and [complex] = 0-50 μM.

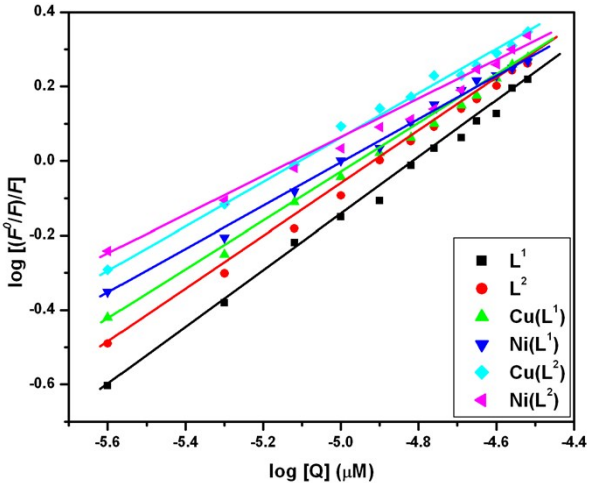

Fig. S14 Scatchard plot of the fluorescence titrations of the Schiff bases and their metal complexes with BSA in Tris-HCl buffer.

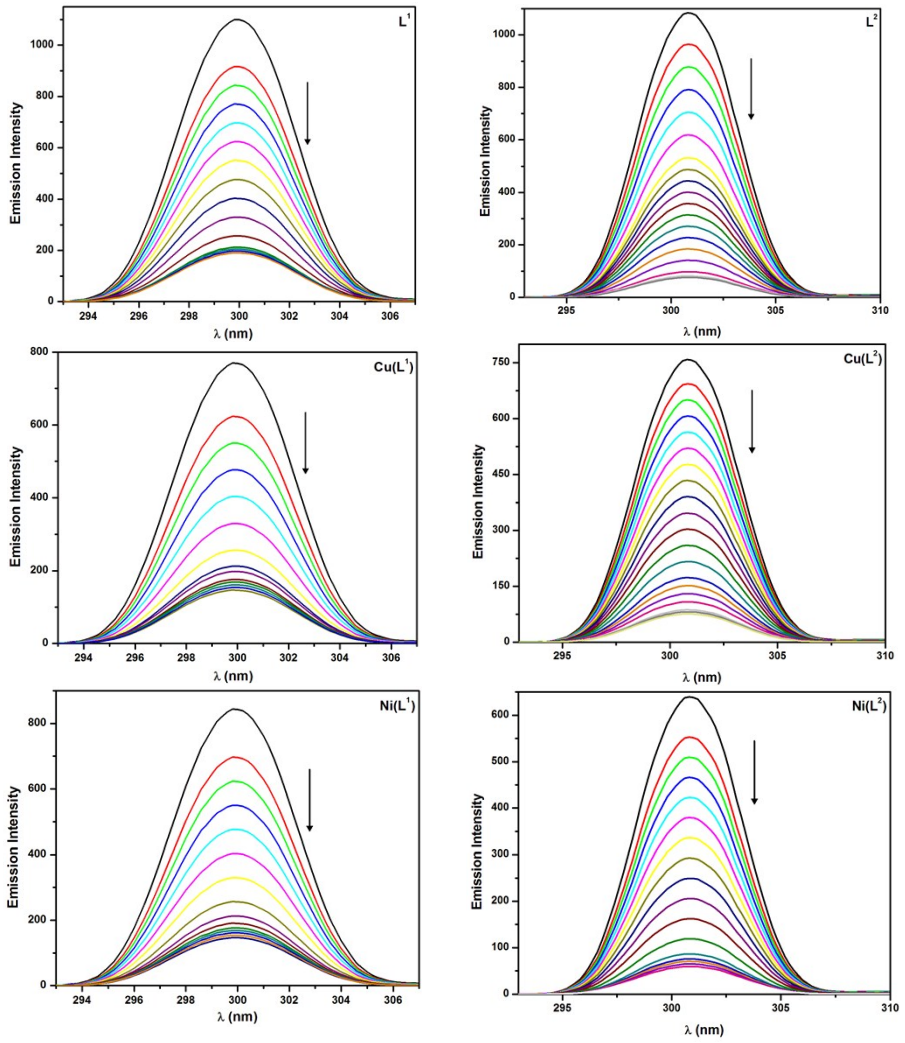

Fig. S15 Synchronous spectra of BSA in the presence of increasing amounts of the Schiff bases and their metal complexes at a wavelength difference of $\Delta\lambda$ = 15 nm. (The arrow shows the emission intensity decreases upon the increase in concentration of the compounds).

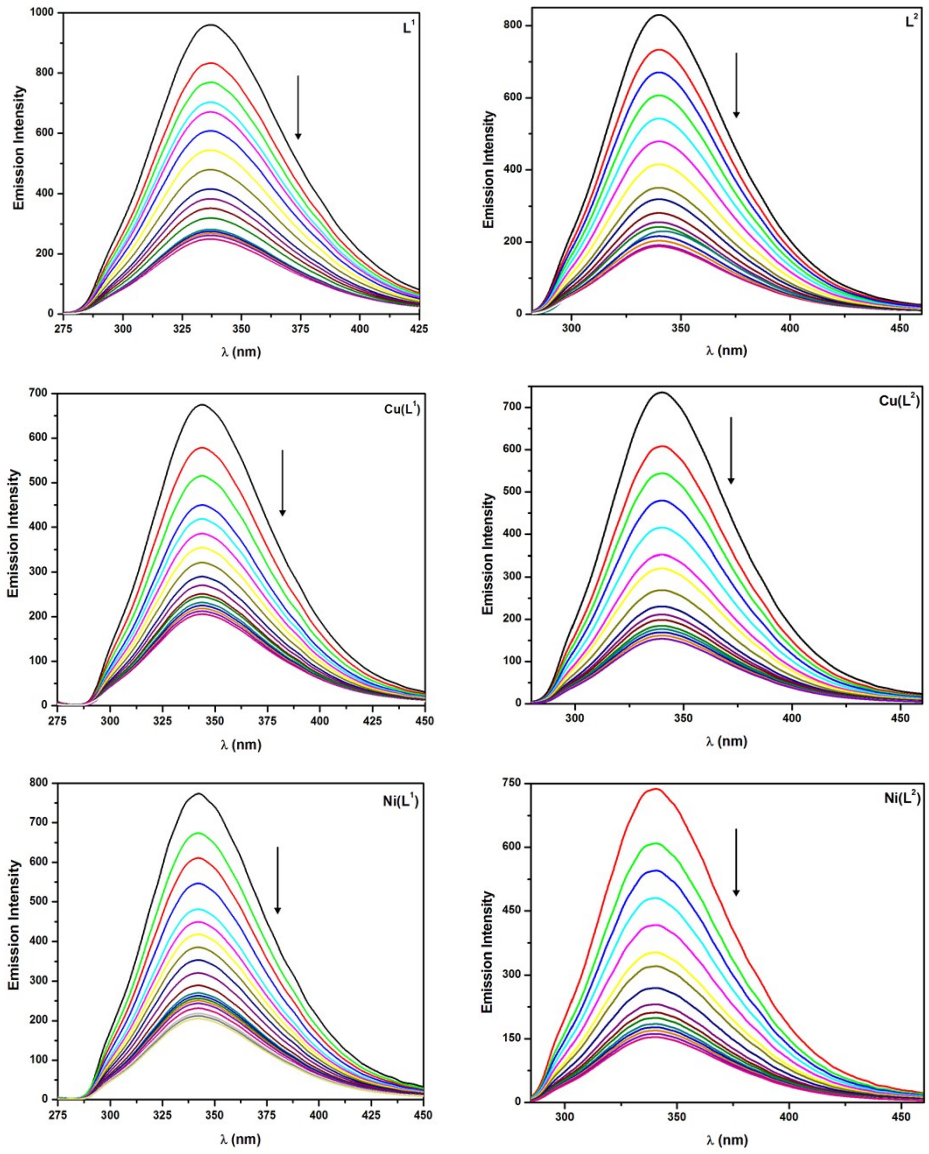

Fig. S16 Synchronous spectra of BSA in the presence of increasing amounts of the Schiff bases and their metal complexes at a wavelength difference of $\Delta\lambda$ = 60 nm. (The arrow shows the emission intensity decreases upon the increase in concentration of the compounds).

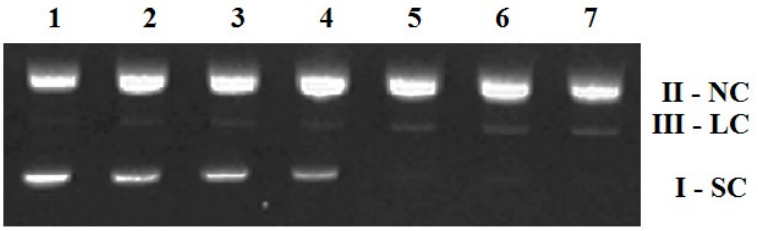

Fig. S17 Agarose gel showing cleavage of pUC19 DNA incubated by Ni(L^1) in Tris–HCl buffer (pH = 7.2) at 37ºC for 1 h. Lane 1: DNA control; Lane 2: 2.5 μM Ni(L^1) + DNA; Lane 3: 5.0 μM Ni(L^1) + DNA; Lane 4: 7.5 μM Ni(L^1) + DNA; Lane 5: 10.0 μM Ni(L^1) + DNA; Lane 6: 12.5 μM Ni(L^1) + DNA; Lane 7: 15.0 μM Ni(L^1) + DNA.

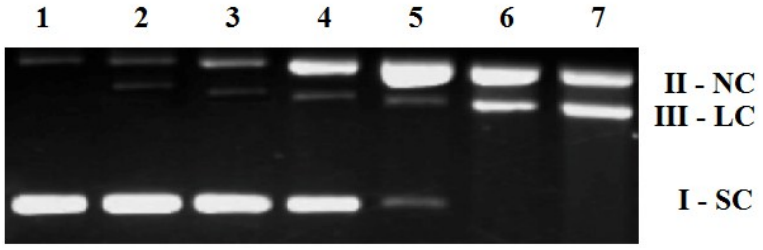

Fig. S18 Agarose gel showing cleavage of pUC19 DNA incubated by Cu(L^2) in Tris–HCl buffer (pH = 7.2) at 37ºC for 1 h. Lane 1: DNA control; Lane 2: 2.5 μM Cu(L^2) + DNA; Lane 3: 5.0 μM Cu(L^2) + DNA; Lane 4: 7.5 μM Cu(L^2) + DNA; Lane 5: 10.0 μM Cu(L^2) + DNA; Lane 6: 12.5 μM Cu(L^2) + DNA; Lane 7: 15.0 μM Cu(L^2) + DNA.

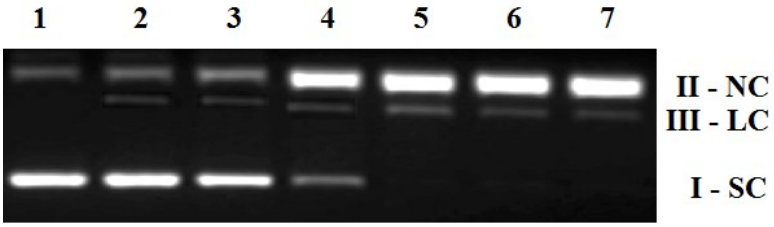

Fig. S19 Agarose gel showing cleavage of pUC19 DNA incubated by Ni(L^2) in Tris–HCl buffer (pH = 7.2) at 37ºC for 1 h. Lane 1: DNA control; Lane 2: 2.5 μM Ni(L^2) + DNA; Lane 3: 5.0 μM Ni(L^2) + DNA; Lane 4: 7.5 μM Ni(L^2) + DNA; Lane 5: 10.0 μM Ni(L^2) + DNA; Lane 6: 12.5 μM Ni(L^2) + DNA; Lane 7: 15.0 μM Ni(L^2) + DNA.

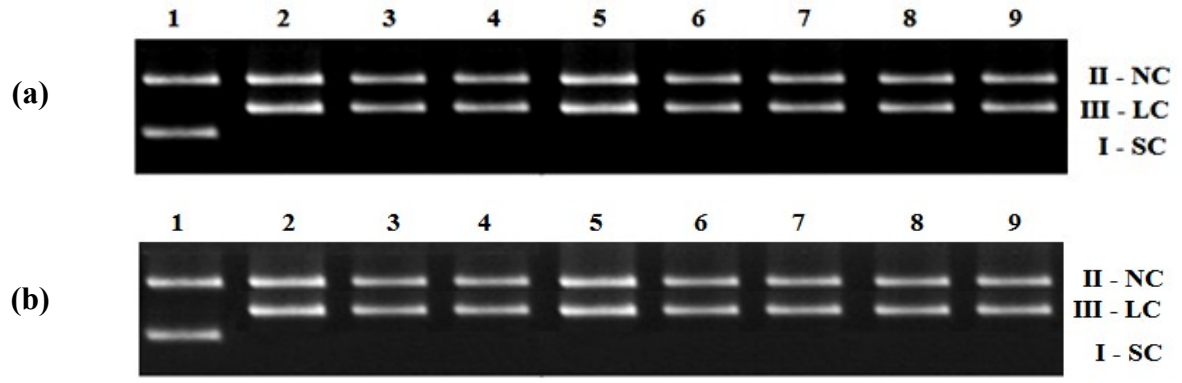

Fig. S20 Agarose gel showing cleavage of pUC19 DNA incubated by complexes with L-Histidine and SOD in Tris–HCl buffer (pH = 7.2) at 37ºC. **(a)** Lane 1: DNA control; Lane 2: Cu(L^1) + L-Histidine (0.25 µM); Lane 3: Ni(L^1) + L-Histidine (0.25 µM); Lane 4: Cu(L^2) + L-Histidine (0.25 µM); Lane 5: Ni(L^2) + L-Histidine (0.25 µM); Lane 6: Cu(L^1) + SOD (4 units); Lane 7: Ni(L^1) + SOD (4 units); Lane 8: Cu(L^2) + SOD (4 units); Lane 9: Ni(L^2) + SOD (4 units); **(b)** Lane 1: DNA control; Lane 2: Cu(L^1) + DMSO (0.1 mM); Lane 3: Ni(L^1) + DMSO (0.1 mM); Lane 4: Cu(L^2) + DMSO (0.1 mM); Lane 5: Ni(L^2) + DMSO (0.1 mM); Lane 6: Cu(L^1) + KI (1 mM); Lane 7: Ni(L^1) + KI (1 mM); Lane 8: Cu(L^2) + KI (1 mM); Lane 9: Ni(L^2) + KI (1 mM).

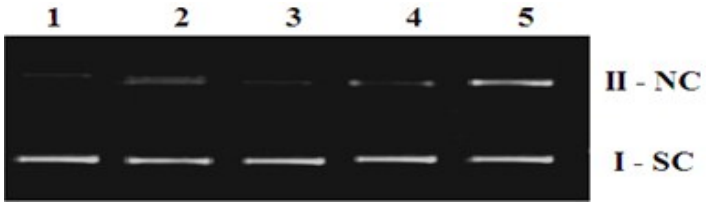

Fig. S21 Agarose gel showing cleavage of pUC19 DNA incubated by complexes (17.5 μM) with EDTA (5 mM) in Tris–HCl buffer (pH = 7.2) at 37ºC for 1 h. Lane 1: DNA control; Lane 2: Cu(L^1) + EDTA; Lane 3: Ni(L^1) + EDTA; Lane 4: Cu(L^2) + EDTA; Lane 5: Ni(L^2) + EDTA.

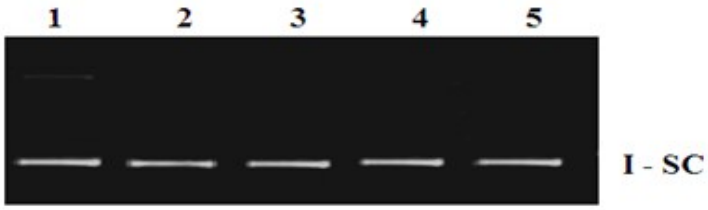

Fig. S22 Agarose gel showing cleavage of pUC19 DNA incubated by complexes with T4 ligase in Tris–HCl buffer (pH = 7.2) at 37ºC for 1 h. Lane 1: DNA control; Lane 2: Cu(L^1) + T4 ligase; Lane 2: Ni(L^1) + T4 ligase; Lane 3: Cu(L^2) + T4 ligase; Lane 4: Ni(L^2) + T4 ligase.

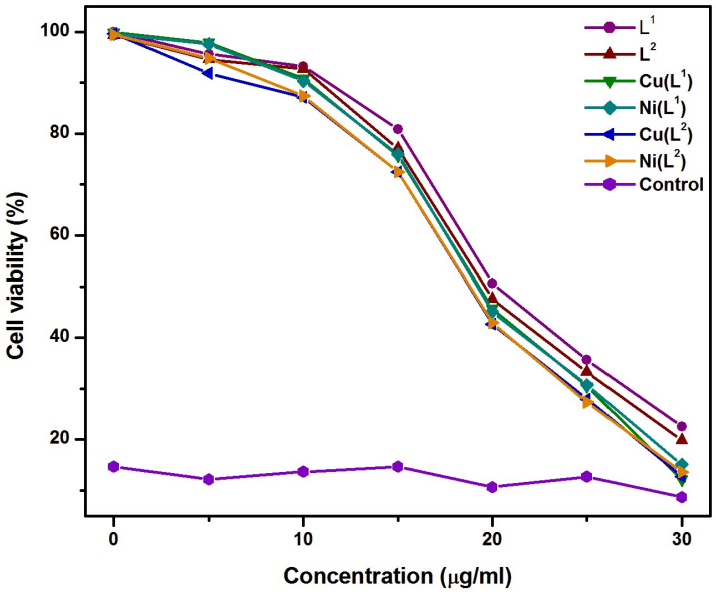

Fig. S23 IC_{50} values of HeLa cells treated with cisplatin, Schiff bases and their complexes.

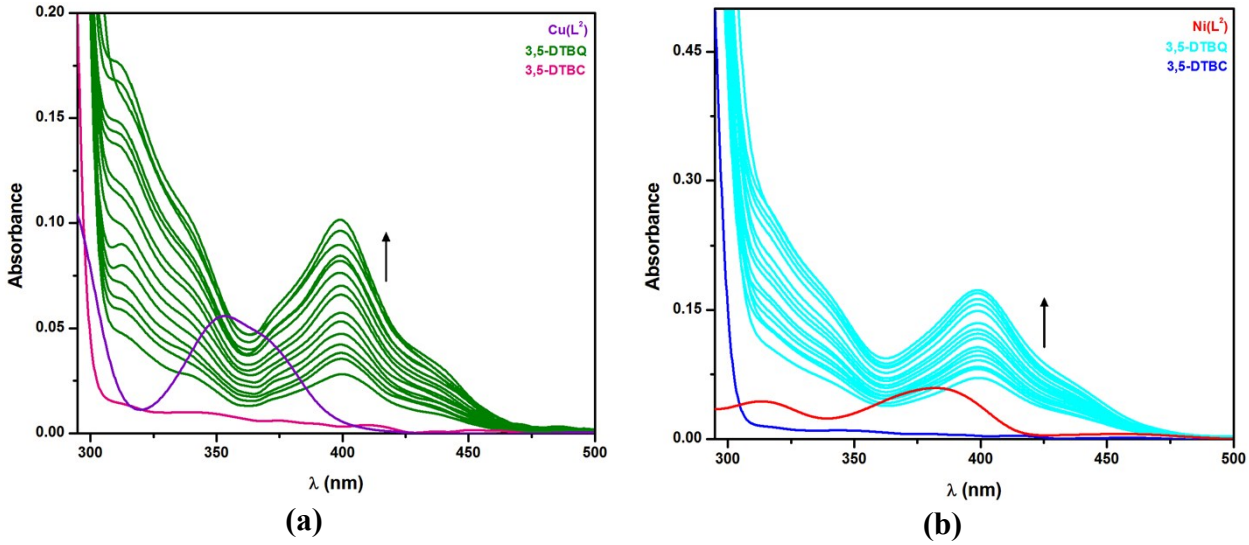

Fig. S24 Catecholase activity by change in time dependent spectral pattern of complexes [(a) $Cu(L^2)$; (b) $Ni(L^2)$] after addition of 3,5 DTBC in acetonitrile medium.

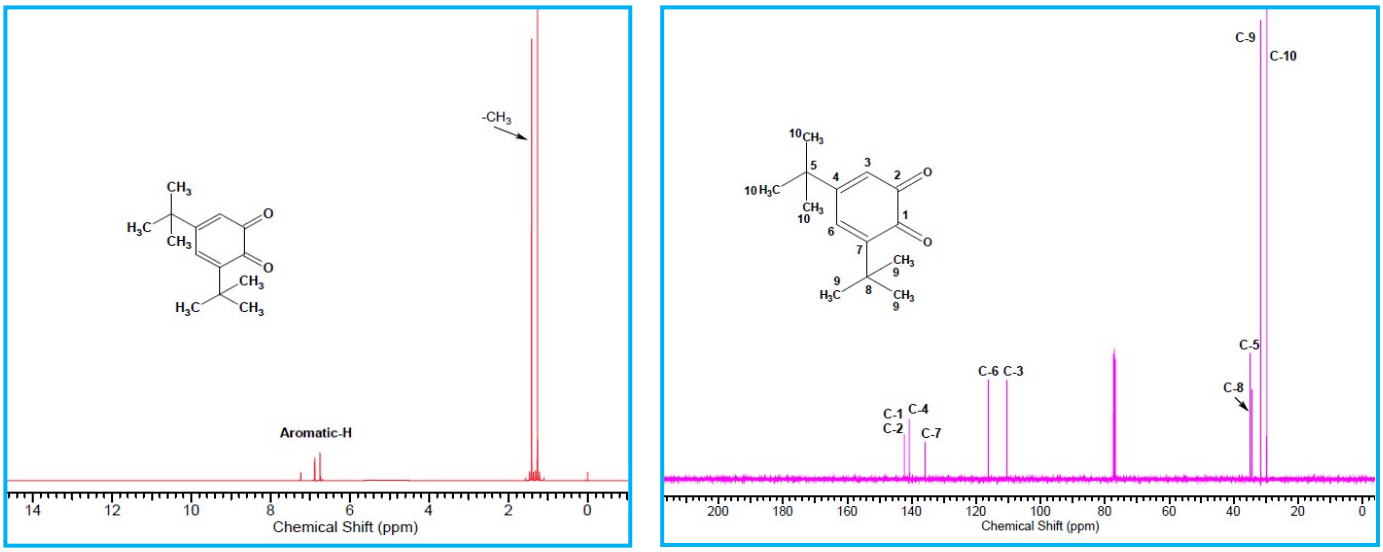

(a) **(b)**

Fig. S25 (a) ^{1}H NMR spectrum of DTBQ; **(b)** ^{13}C NMR spectrum of DTBQ.

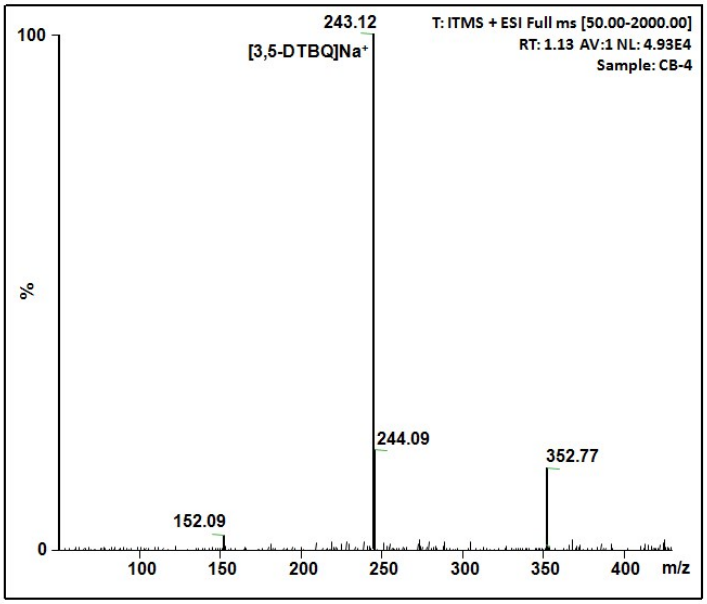

Fig. S26 Electrospray mass spectrum (ESI-MS positive) of 3,5-DTBQ during the reaction of complexes with 3,5-DTBC.

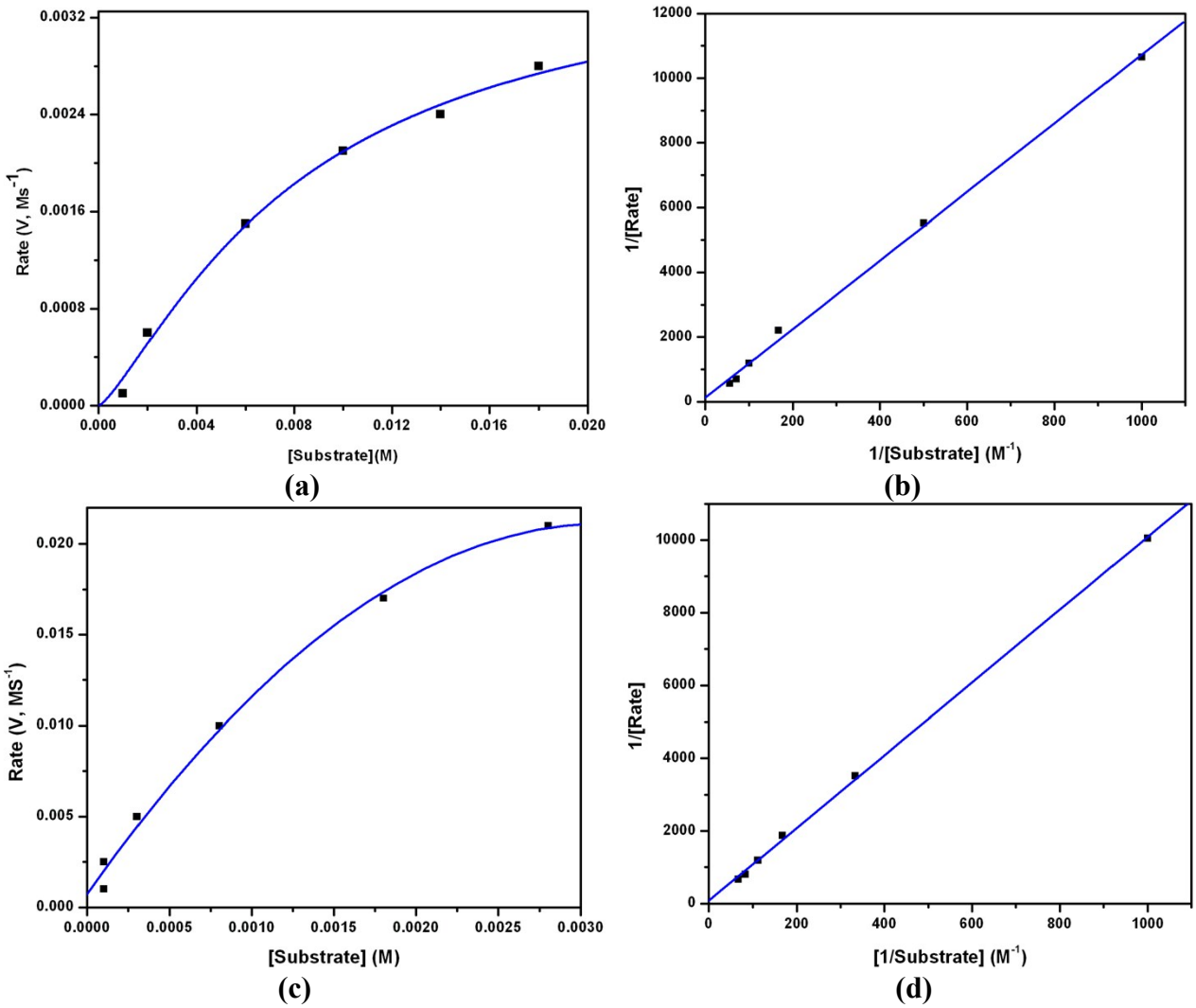

Fig. S27 Plot of rate vs substrate concentration for **(a)** Cu(L^2); **(b)** Lineweaver-Burk plot for Cu(L^2); **(c)** Ni(L^2); **(d)** Lineweaver-Burk plot for Ni(L^2).

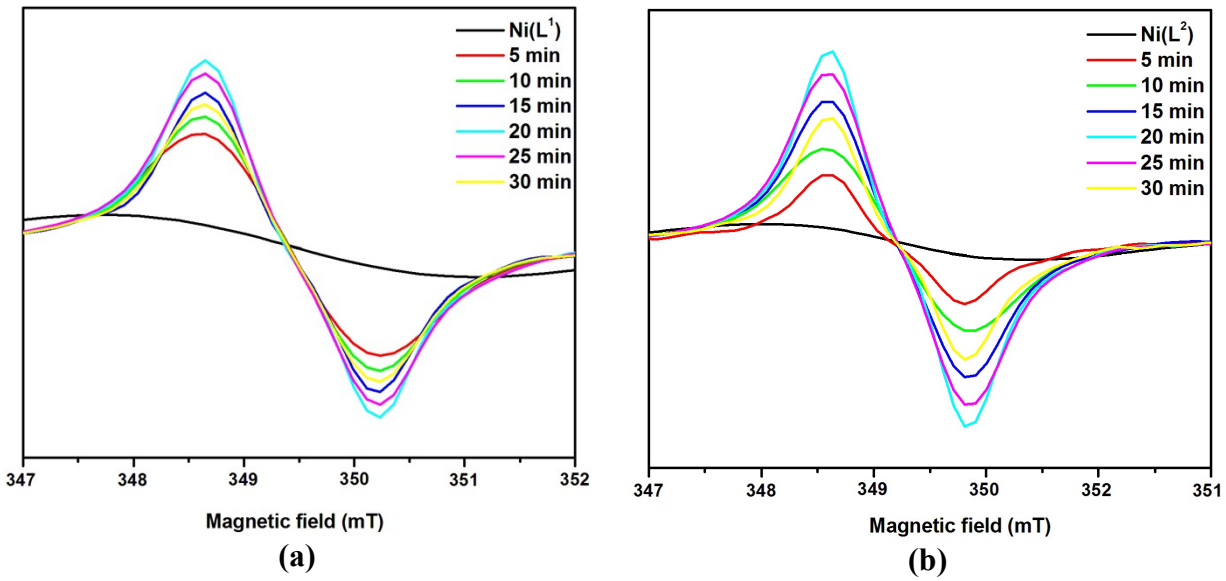

Fig. S28 EPR spectra in different time intervals of acetonitrile solution of complexes [**(a)** Ni(L^1); **(b)** Ni(L^2)] after the addition of 3,5-DTBC at room temperature.

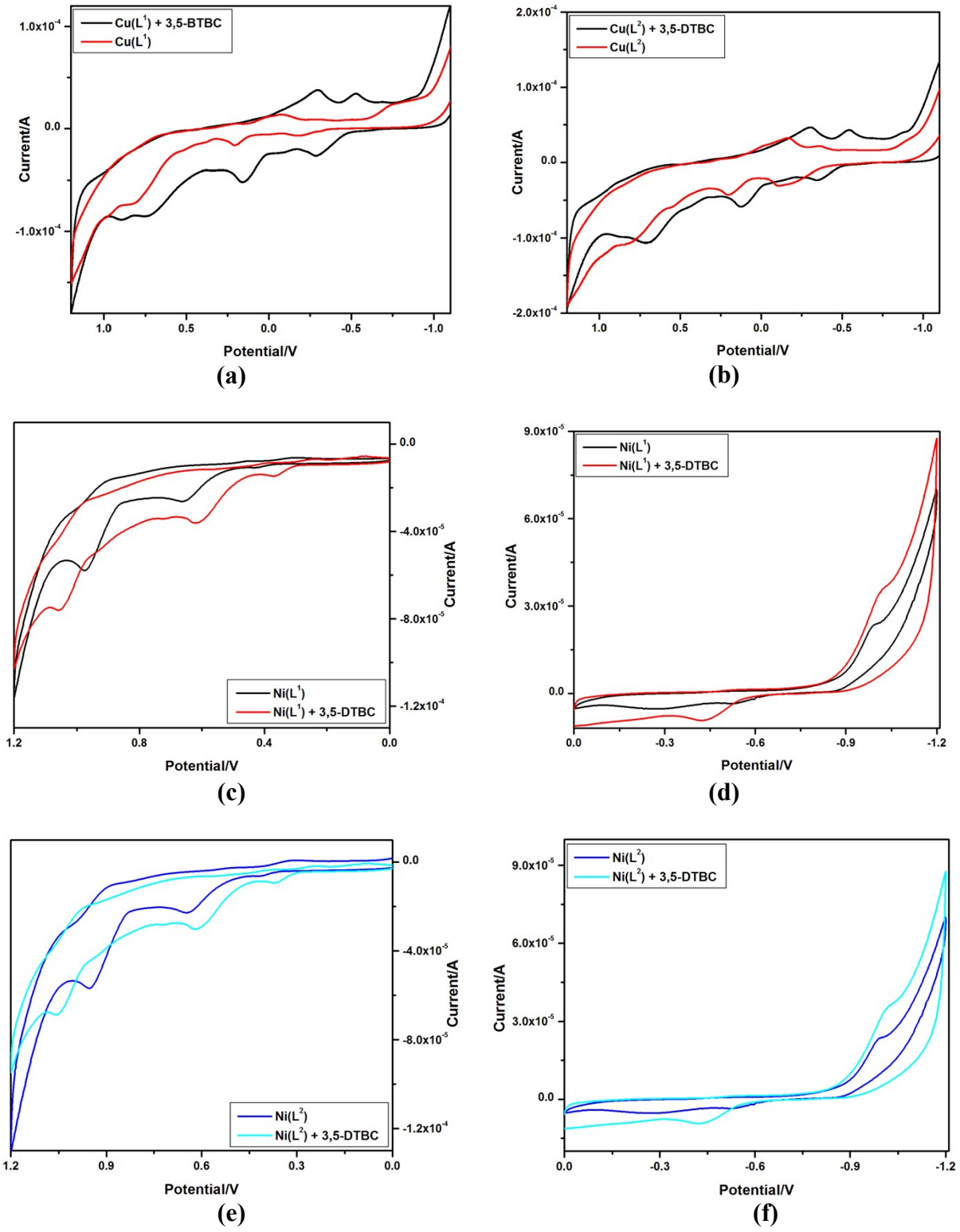

Fig. S29 Cyclic voltammogram of complexes after the addition of 3,5-DTBC solution, **(a)** $Cu(L^1)$; **(b)** $Cu(L^2)$; **(c,d)** $Ni(L^1)$ and **(e,f)** $Ni(L^2)$.

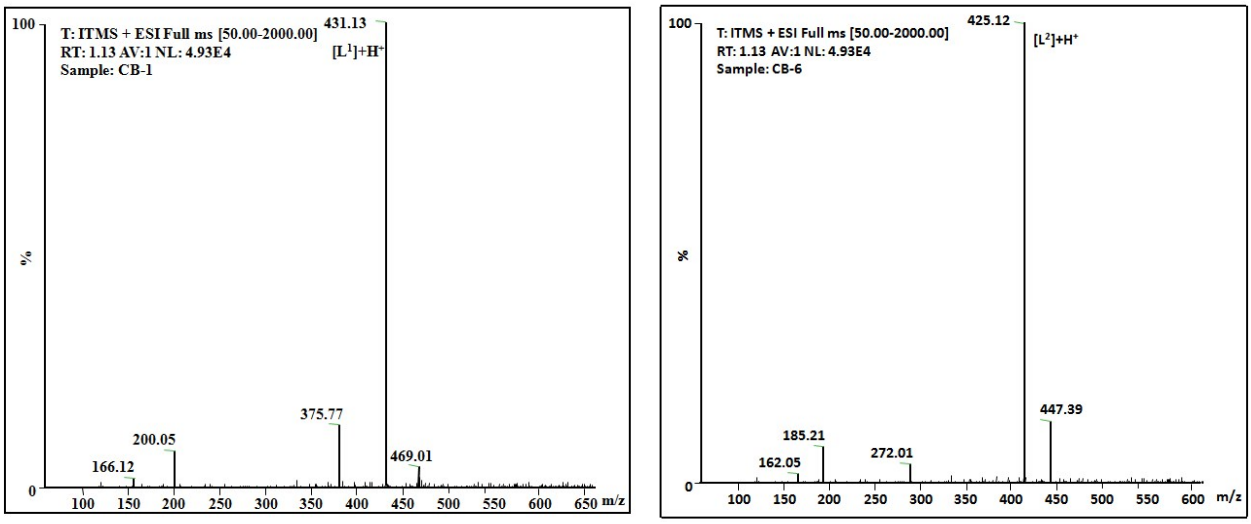

(a) **(b)**

Fig. S30 Electrospray mass spectrum (ESI-MS positive) of, **(a)** L^1; **(b)** L^2 in acetonitrile solvent

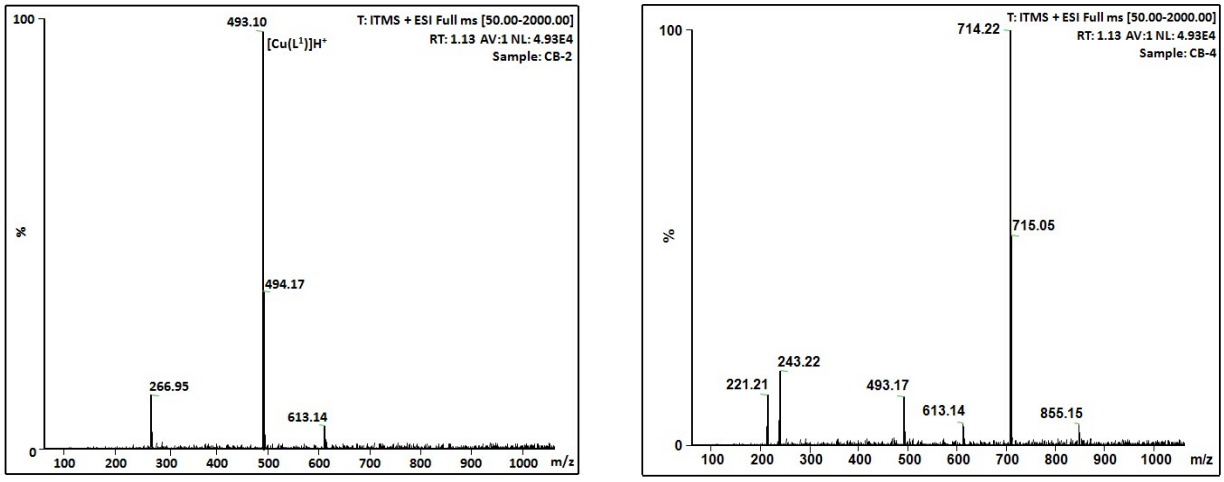

(a) **(b)**

Fig. S31 Electrospray mass spectra (ESI-MS positive) of, **(a)** Cu(L^1); **(b)** 1:100 mixture of Cu(L^1) and 3,5-DTBC, recorded within 5 min of mixing.

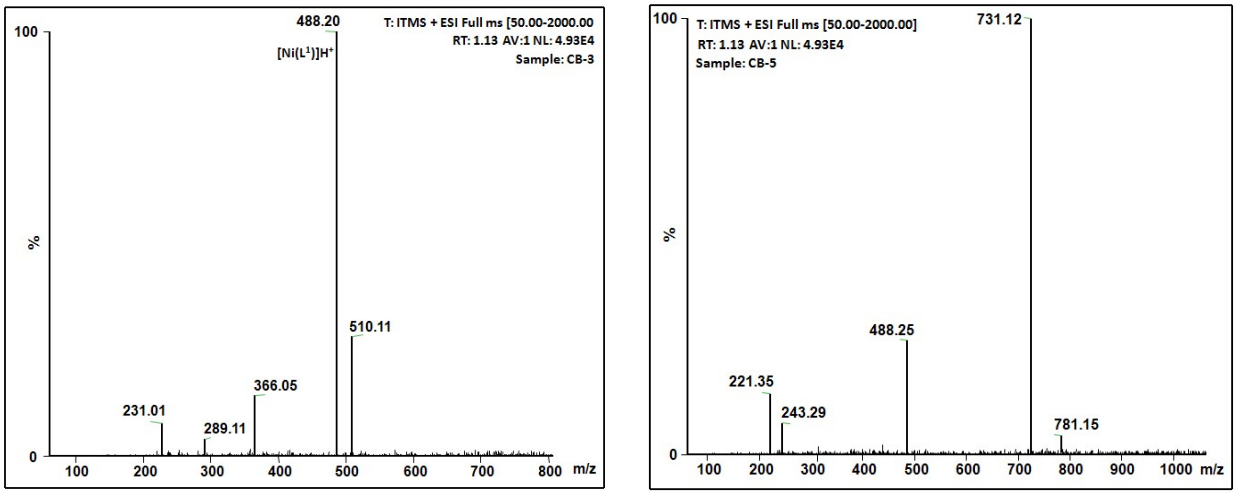

(a) **(b)**

Fig. S32 Electrospray mass spectrum (ESI-MS positive) of, **(a)** Ni(L^1); **(b)** 1:100 mixture of Ni(L^1) and 3,5-DTBC in acetonitrile, recorded within 5 min of mixing.

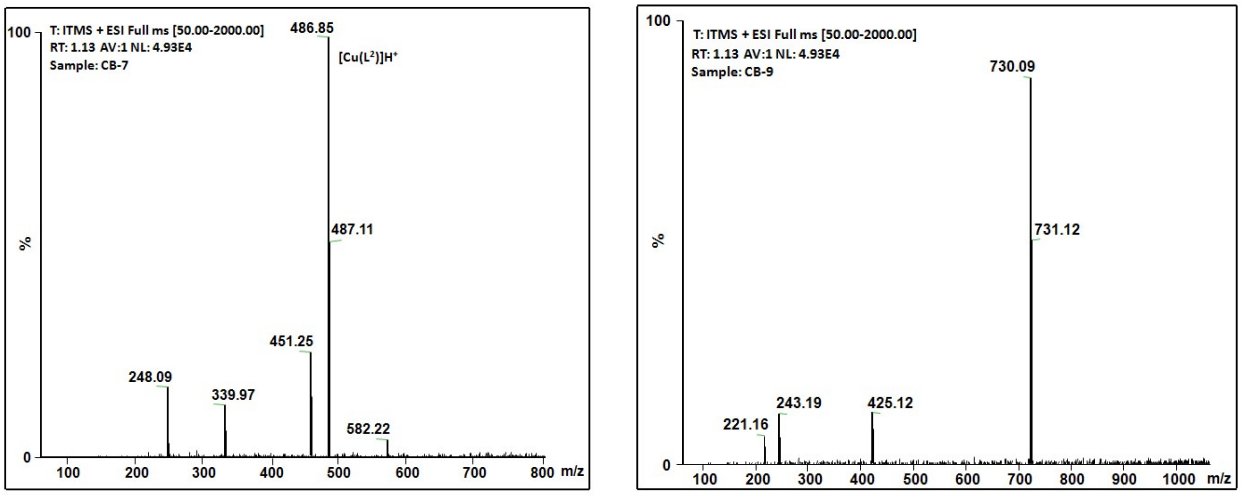

(a) **(b)**

Fig. S33 Electrospray mass spectrum (ESI-MS positive) of, **(a)** Cu(L^2); **(b)** 1:100 mixture of Cu(L^2) and 3,5-DTBC in acetonitrile, recorded within 5 min of mixing.

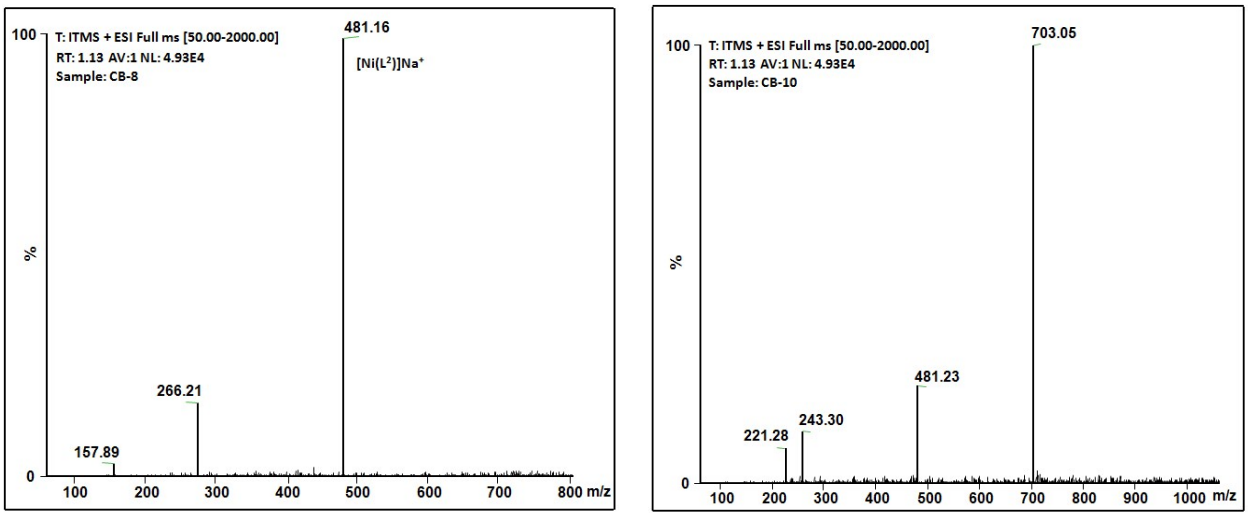

(a) **(b)**

Fig. S34 Electrospray mass spectrum (ESI-MS positive) of, **(a)** Ni(L^2); **(b)** 1:100 mixture of Ni(L^2) and 3,5-DTBC in acetonitrile, recorded within 5 min of mixing.

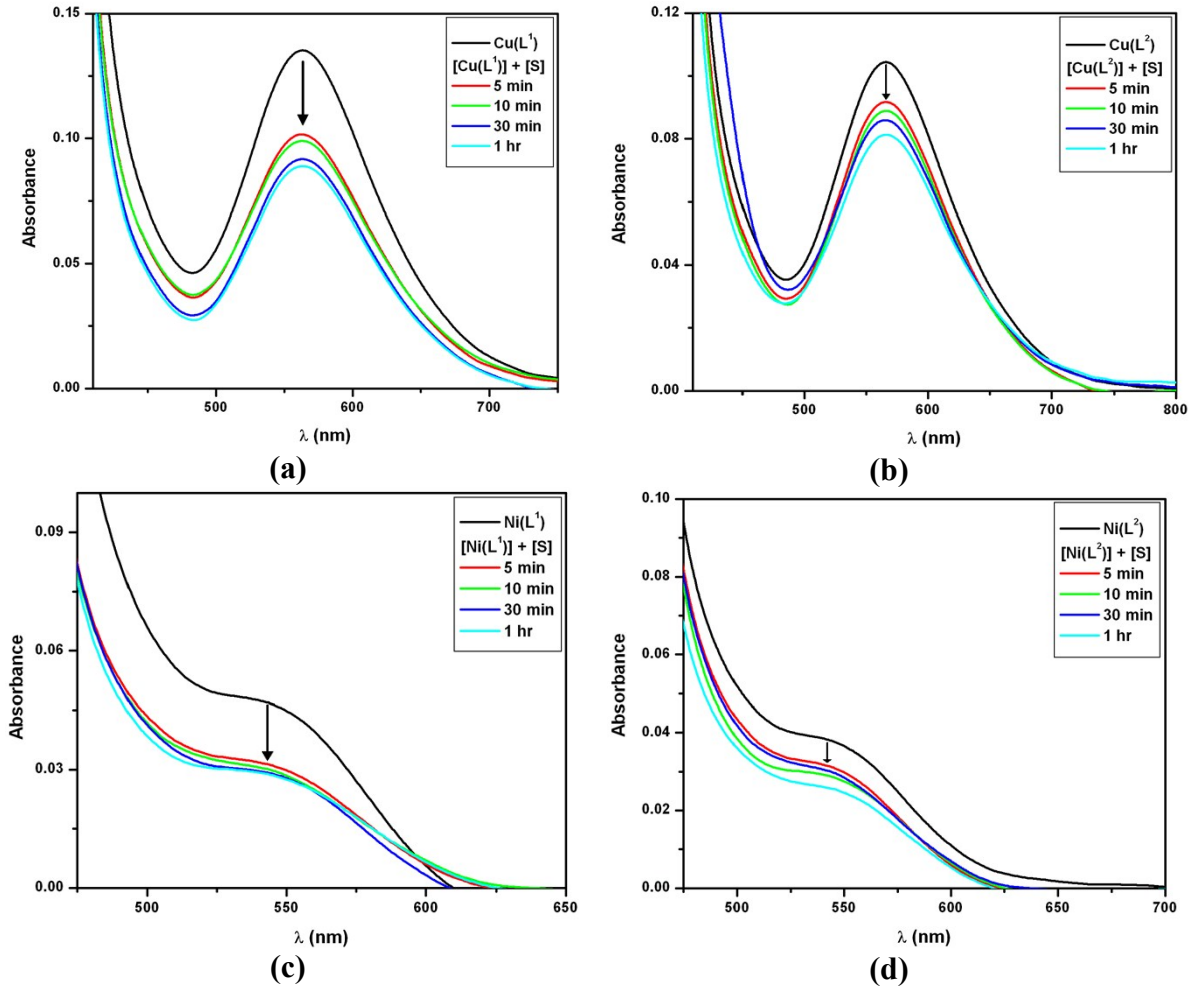

Fig. S35 UV-Vis spectra (500 - 900 nm) of complexes, **(a)** $Cu(L^1)$; **(b)** $Cu(L^2)$; **(c)** $Ni(L^1)$; **(d)** $Ni(L^2)$ with addition of 3,5-DTBC.

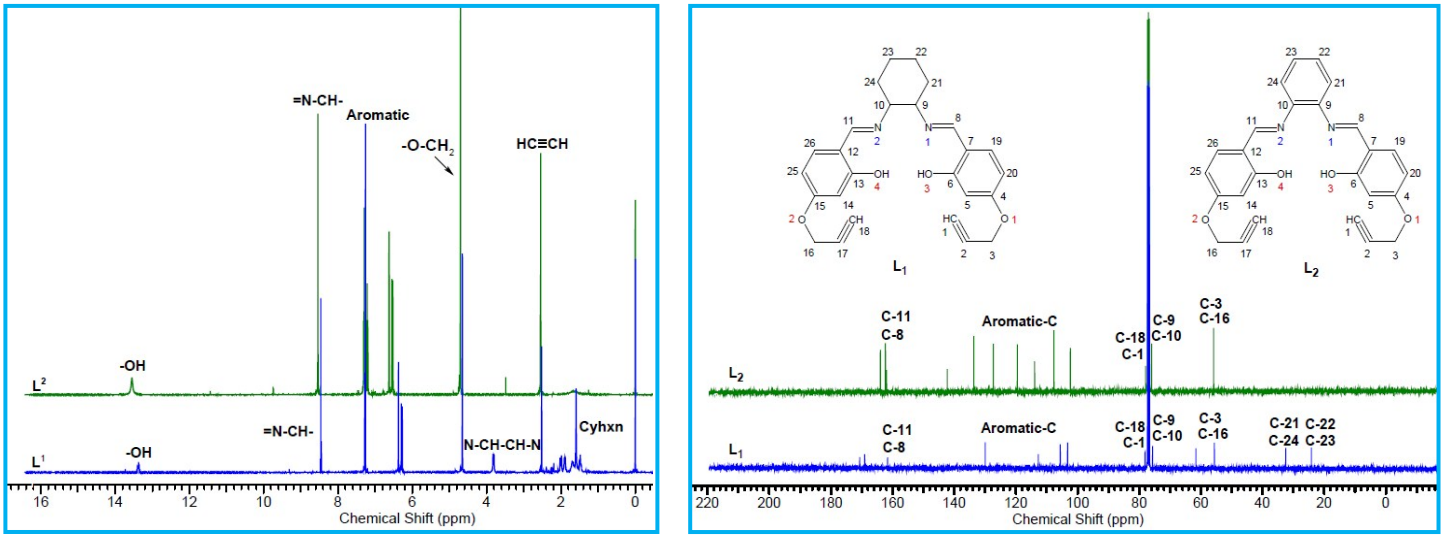

(a) **(b)**

Fig. S36 (a) ^{1}H NMR spectra of Schiff bases; **(b)** ^{13}C NMR spectra of Schiff bases.

Spectrophotometric detection of H2O2 in the oxidation reaction

Reaction mixtures were prepared as in the kinetic experiments. After 1 h of the reaction an equal volume of water was added and the quinone formed was extracted three times with dichloromethane. The aqueous layer was acidified with H_2SO_4 to pH = 2 to stop further oxidation, and 1 mL of a 10% solution of KI and three drops of 3% solution of ammonium molybdate were added. In the presence of hydrogen peroxide occurs the reaction $H_2O_2 + 2I^- + 2H^+ \rightarrow 2H_2O + I_2$, and with an excess of iodide ions, the tri-iodide ion is formed according to the reaction $I_2\,(aq) + I^- \rightarrow I^{3-}$. The formation of I^{3-} was monitored spectrophotometrically due to the development of the characteristic I^{3-} band (λ = 353 nm).

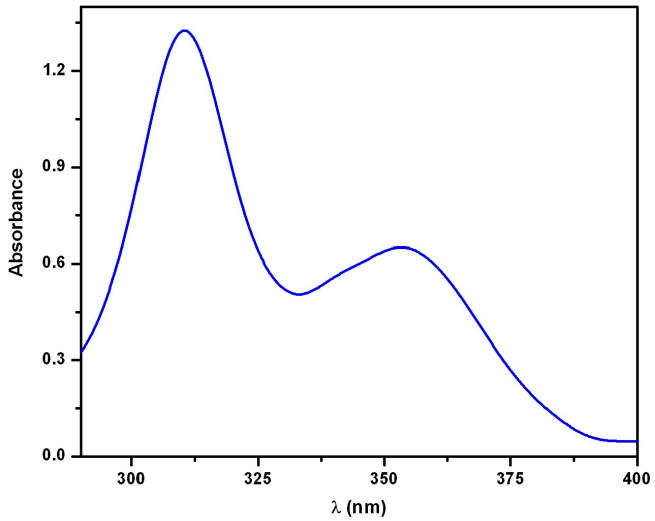

Fig. S37 Electronic spectra of the formation of $I3^-$ ion in presence of H_2O_2.

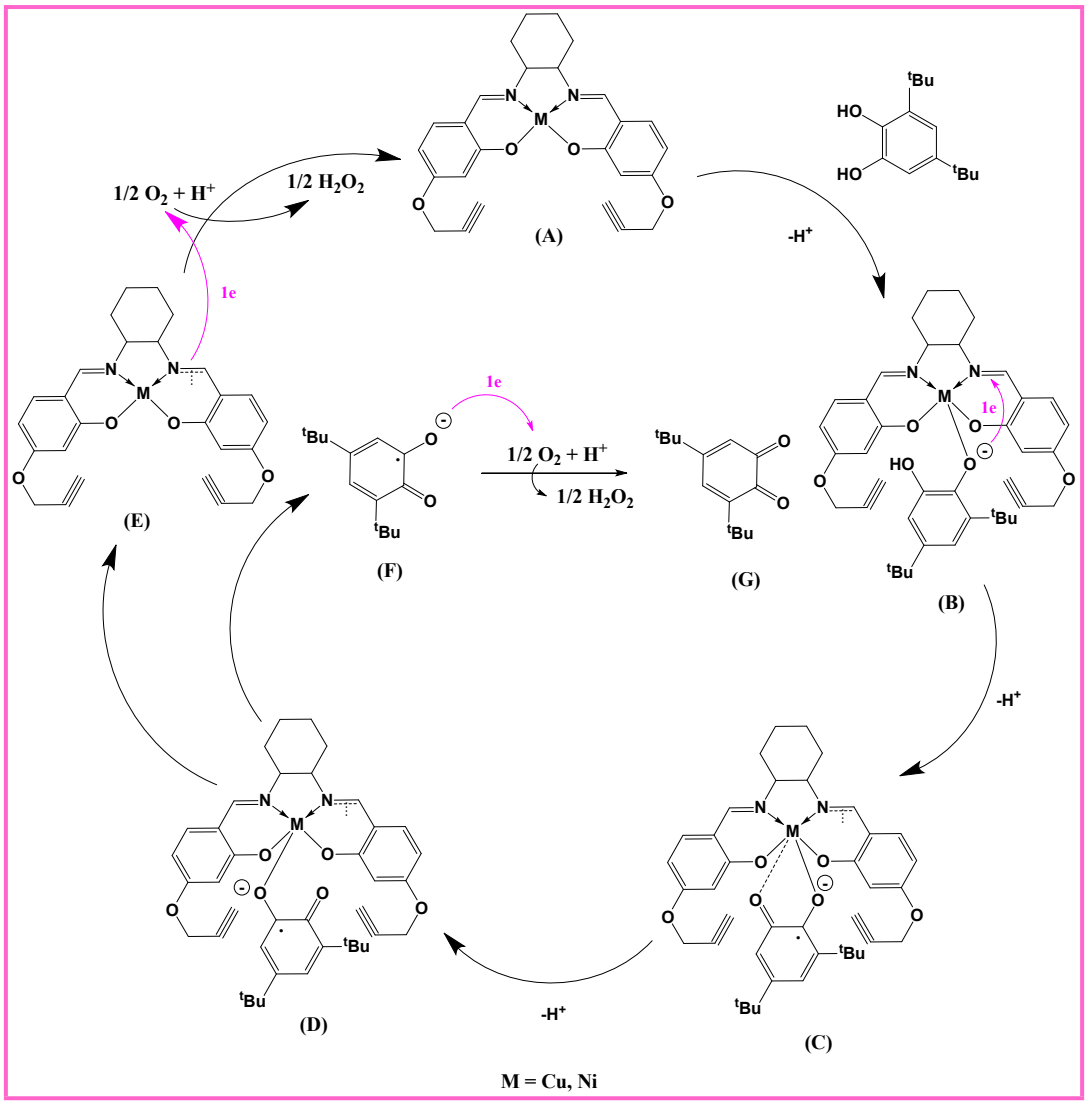

Scheme S1 Probable catalytic cycle of oxidation of 3,5 DTBC by M(L^1) complexes.

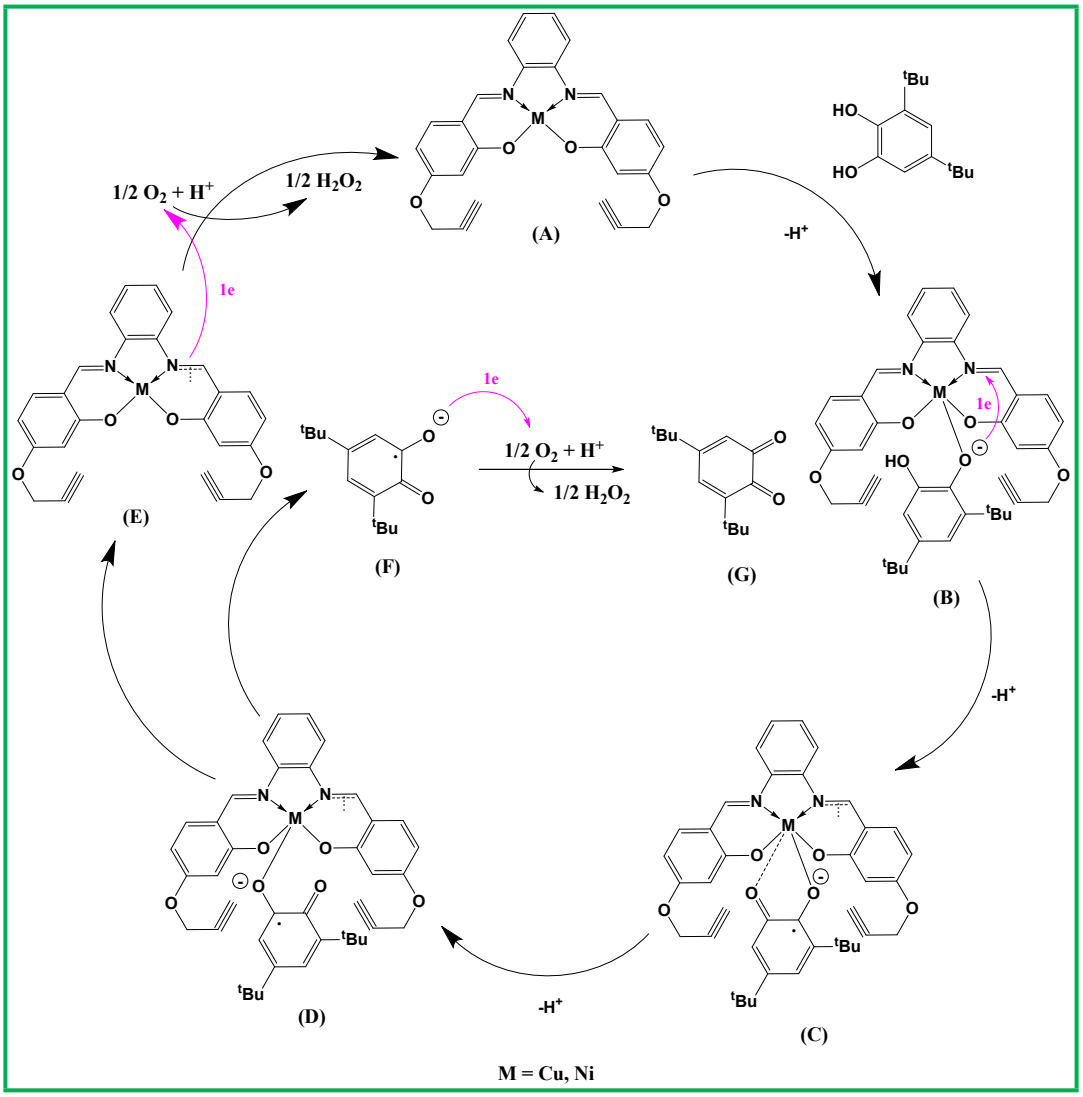

Scheme S2 Probable catalytic cycle of oxidation of 3,5 DTBC by M(L^2) complexes.

Table S1 Spin Hamiltonian parameters of Cu(L^1) and Cu(L^2) in acetonitrile.

	Hyperfine constant 10^{-4} (cm^{-1})										
	$A_{\parallel}$	$A_{\perp}$	$g_{\parallel}$	$g_{\perp}$	$g_{\parallel}/A_{\parallel}$	$K_{\parallel}$	$K_{\perp}$	G	α^2	β^2	γ^2
Cu(L^1)	199	65.7	2.27	2.13	114	0.69	1.42	2.10	1.43	0.48	0.99
Cu(L^2)	202	54.3	2.24	2.11	110	1.77	1.92	2.22	1.44	1.22	1.33

Table S2 Selected bond lengths (Å) and bond angles (◦) for Cu(L^1).

Bond length	Å	Bond angles	◦
Cu(1)-O(2)	1.887(2)	O(2)-Cu(1)-O(3)	87.86(9)
Cu(1)-O(3)	1.888(2)	O(2)-Cu(1)-N(2)	94.69(11)
Cu(1)-N(2)	1.923(3)	O(3)-Cu(1)-N(2)	174.92(12)
Cu(1)-N(1)	1.927(3)	O(2)-Cu(1)-N(1)	175.65(11)
O(1)-C(7)	1.362(4)	O(3)-Cu(1)-N(1)	93.47(11)
O(1)-C(8)	1.396(5)	N(2)-Cu(1)-N(1)	84.30(12)
O(2)-C(12)	1.299(4)	C(12)-O(2)-Cu(1)	126.3(2)
O(3)-C(19)	1.310(4)	C(19)-O(3)-Cu(1)	126.3(2)
O(4)-C(21)	1.366(4)	C(17)-N(1)-Cu(1)	126.0(2)
O(4)-C(22)	1.409(5)	C(1)-N(1)-Cu(1)	111.0(2)
N(1)-C(17)	1.273(4)	C(3)-N(2)-Cu(1)	125.1(2)
N(1)-C(1)	1.467(4)	C(2)-N(2)-Cu(1)	112.1(2)
N(2)-C(3)	1.280(5)	Torsion angles	◦
N(2)-C(2)	1.488(4)	C(1)-N(1)-Cu(1)-O(3)	166.69
C(14)-C(15)	1.449(7)	C(2)-N(2)-Cu(1)-O(2)	175.32
C(15)-C(16)	1.512(5)	N(1)-C(1)-C(2)-N(2)	46.24
C(17)-C(18)	1.424(5)	C(12)-O(3)-Cu(1)-O(2)	179.22
		C(19)-O(2)-Cu(1)-O(3)	169.60

Symmetry codes: (i) x,y,z; (ii) 1/2-x,1/2+y,1/2-z; (iii) 1/2+x,1/2-y,1/2+z; (iv) -x,-y,-z.

Table S3 Selected bond lengths (Å) and bond angles (◦) for Ni(L^1).

Bond length	Å	Bond angles	◦
N(1)-Ni(1)	1.850(2)	C(17)-N(1)-Ni(1)	126.00(18)
N(2)-Ni(1)	1.854(2)	C(16)-N(1)-Ni(1)	111.98(17)
O(1)-Ni(1)	1.8416(17)	C(10)-N(2)-Ni(1)	126.09(18)
O(2)-Ni(1)	1.8314(18)	C(11)-N(2)-Ni(1)	112.77(18)
C(3)-O(3)	1.431(3)	O(2)-Ni(1)-O(1)	83.37(8)
C(4)-O(3)	1.371(3)	O(2)-Ni(1)-N(2)	178.25(9)
C(8)-O(1)	1.311(3)	O(1)-Ni(1)-N(2)	94.99(9)
C(10)-N(2)	1.289(3)	N(1)-Ni(1)-N(2)	86.55(9)
C(11)-N(2)	1.483(4)	O(1)-Ni(1)-N(1)	178.12(9)
C(16)-N(1)	1.492(3)	O(2)-Ni(1)-N(2)	178.25(9)
C(17)-N(1)	1.291(3)	Torsion angles	◦
C(21)-O(4)	1.372(3)	C(17)-N(1)-Ni(1)-O(2)	8.3(3)
C(23)-O(2)	1.309(3)	C(16)-N(1)-Ni(1)-O(1)	158(3)
C(24)-O(4)	1.421(3)	C(16)-N(1)-Ni(1)-N(2)	12.8(2)
C(23)-O(2)	1.309(3)	C(11)-N(2)-Ni(1)-O(2)	173(3)
C(8)-O(1)	1.311(3)	C(10)-N(2)-Ni(1)-O(1)	10.5(3)
		C(11)-N(2)-Ni(1)-N(1)	12.6(2)

Symmetry codes: (i) x,y,z; (ii) 1/2-x,1/2+y,1/2-z; (iii) -x,-y,-z; (iv) 1/2+x,1/2-y,1/2+z.

Table S4 Electronic absorption value of complexes and complexes with CT-DNA in buffer medium.

	Complex (λ_{max}) (nm)	Complex + CT-DNA (λ_{max}) (nm)
$Cu(L^1)$	295	292
$Ni(L^1)$	277	274
$Cu(L^2)$	297	289
$Ni(L^2)$	279	275

Table S5 Fluorescence lifetime of EB-DNA and with increasing amounts of metal complexes.

Complexes	Conc. (μM)	τ_1 (ns)	τ_2 (ns)	τ_3 (ns)	α_1	α_2	α_3	τ (ns)	χ^2
EB-DNA	-	19.26	20.63	21.54	6.95	7.25	7.82	20.55	1.059
EB-DNA + Cu(L^1)	50	14.89	15.34	16.02	5.62	6.42	7.11	15.46	1.142
	100	13.96	15.18	15.91	5.29	6.07	6.73	15.14	1.006
	150	13.12	14.89	15.58	5.08	5.86	6.37	14.67	1.098
	200	12.10	14.12	15.23	3.78	4.69	5.48	14.12	1.284
	250	11.25	12.96	14.38	3.17	4.05	4.89	13.21	1.147
EB-DNA + Ni(L^1)	50	15.05	15.47	16.23	5.89	6.76	7.29	15.63	1.257
	100	14.20	15.28	15.67	5.46	6.35	6.95	15.14	1.084
	150	13.01	14.17	15.38	4.83	5.42	6.02	14.75	1.254
	200	13.41	14.68	15.53	5.21	5.84	6.36	14.66	1.195
	250	12.75	13.86	14.97	4.52	5.14	5.62	13.99	1.224
EB-DNA + Cu(L^2)	50	14.62	15.81	16.05	5.72	7.15	7.46	15.58	1.192
	100	13.76	14.98	15.83	5.56	6.29	6.67	14.96	1.240
	150	11.72	13.81	15.11	3.40	4.43	5.24	14.90	1.019
	200	11.42	13.13	14.67	3.22	4.19	5.03	13.44	1.171
	250	10.48	12.61	14.26	2.67	3.38	4.42	12.94	1.232
EB-DNA + Ni(L^2)	50	14.25	15.46	16.31	5.56	6.35	7.09	15.47	1.129
	100	14.08	14.92	15.27	2.25	6.02	6.51	14.81	1.252
	150	13.18	14.01	15.35	4.87	5.56	6.18	14.23	1.010
	200	12.63	13.54	14.88	4.15	4.96	5.16	13.82	1.286
	250	10.52	13.05	14.47	2.29	3.85	4.66	13.16	1.194

Table S6 Cytotoxic effect (IC_{50}, μM) of ligands and metal complexes against HeLa cell.

S. No.	Compounds	IC_{50} (μM)
1	L^1	22.52 ± 0.49
2	L^2	19.86 ± 0.62
3	$Cu(L^1)$	12.15 ± 0.04
4	$Ni(L^1)$	15.11 ± 0.13
5	$Cu(L^2)$	11.02 ± 0.16
6	$Ni(L^2)$	13.63 ± 0.09
7	Cisplatin	8.67 ± 0.04

Table S7 Kinetic Data for Catecholase-like Activity of Different Copper and Nickel Complexes.

	Catalyst	Solvent	k_{cat} (h^{-1})	Ref.
	Cu(II) Compounds			
(1)	[N-mesityl-2-(pyridine-2-ylmethylamino)-acetamide]$Cu(NO_3)_2.2H_2O$	methanol	6.00	S5
	[[N-(2,6-diethylphenyl)-2-[(pyridin-2-ylmethyl)amino]acetamide]$Cu(NO_3)(OH_2)]NO_3.H_2O$	methanol	3.00	S5
	[N-mesityl-2-(pyridine-2-ylmethylamino)acetamide]$CuCl_2.H_2O$	methanol	0.20	S5
(2)	$[CuL(\mu_{1,5}\text{-dca})]_n$	acetonitrile	27.6	S6
(3)	$Cu(L^1)$	acetonitrile	234.60	This work
(4)	$Cu(L^2)$	acetonitrile	225.40	This work
	Ni(II) Compounds			
(5)	$[NiL^2(H_2O)_3](NO_3)_2$	methanol	52.60	S7
	$[NiL^3(H_2O)_3](NO_3)_2$	methanol	129.00	S7
(6)	[Ni(L)]	acetonitrile	140.72	S8
(7)	$Ni(L^1)$	acetonitrile	168.00	This work
(8)	$Ni(L^2)$	acetonitrile	84.40	This work

Table S8 ESI-mass spectral data for the metal complexes.

	Species	*m/z*
$Cu(L^1)$	$[CuL^1]H^+$	493.10
	$[CuL^1(3,5\text{-DTBC})]H^+$	714.22
	$[3,5\text{-DTBQ}]H^+$	221.21
	$[3,5\text{-DTBQ}]Na^+$	243.22
$Ni(L^1)$	$[NiL^1]H^+$	488.20
	$[NiL^1]Na^+$	510.11
	$[NiL^1(3,5\text{-DTBC})]H^+$	731.12
	$[3,5\text{-DTBQ}]H^+$	221.35
	$[3,5\text{-DTBQ}]Na^+$	243.29
$Cu(L^2)$	$[CuL^2]H^+$	486.85
	$[CuL^2]Na^+$	447.39
	$[NiL^1(3,5\text{-DTBC})]H^+$	730.09
	$[3,5\text{-DTBQ}]H^+$	221.16
	$[3,5\text{-DTBQ}]Na^+$	243.19
$Ni(L^2)$	$[(NiL^2)]Na^+$	481.16
	$[NiL^2(3,5\text{-DTBC})]H^+$	703.05
	$[3,5\text{-DTBQ}]H^+$	221.28
	$[3,5\text{-DTBQ}]Na^+$	243.30

Table S9 Selected bond lengths (Å) and bond angles (◦) for Cu(L^1) and Cu(L^2) at DFT-B3LYP level.

	Cu(L^1)	Cu(L^2)		Cu(L^1)	Cu(L^2)
Bond length	Å		Bond angles	◦	
Cu(1)-O(2)	1.89120	1.90254	O(2)-Cu(1)-O(3)	92.74962	92.98251
Cu(1)-O(3)	1.89281	1.90925	O(2)-Cu(1)-N(2)	93.98847	93.99899
Cu(1)-N(2)	1.93939	1.94062	O(3)-Cu(1)-N(2)	160.72945	160.85341
Cu(1)-N(1)	1.93780	1.93982	O(2)-Cu(1)-N(1)	160.99740	160.99865
O(1)-C(7)	1.36322	1.36985	O(3)-Cu(1)-N(1)	94.07386	94.10256
O(1)-C(8)	1.42935	1.43025	N(2)-Cu(1)-N(1)	85.28352	85.28956
O(2)-C(12)	1.29539	1.29991	C(12)-O(2)-Cu(1)	127.79600	127.87542
O(3)-C(19)	1.29480	2.29856	C(19)-O(3)-Cu(1)	127.83350	127.83954
O(4)-C(21)	1.36322	1.36894	C(17)-N(1)-Cu(1)	125.35618	125.35895
O(4)-C(22)	1.42936	1.43011	C(1)-N(1)-Cu(1)	111.43473	111.43854
N(1)-C(17)	1.30167	1.30854	C(3)-N(2)-Cu(1)	125.41092	125.42982
N(1)-C(1)	1.46946	1.47091	C(2)-N(2)-Cu(1)	111.39585	111.39812
N(2)-C(3)	1.30153	1.30481	Torsion angles	◦	
N(2)-C(2)	1.46963	1.47021	C(1)-N(1)-Cu(1)-O(3)	174.80389	174.81024
C(14)-C(15)	1.53347	1.53569	C(2)-N(2)-Cu(1)-O(2)	175.05497	175.09125
C(15)-C(16)	1.53710	1.53960	N(1)-C(1)-C(2)-N(2)	47.14686	47.14923
C(17)-C(18)	1.42436	1.42725	C(12)-O(3)-Cu(1)-O(2)	179.95241	179.96451
			C(19)-O(2)-Cu(1)-O(3)	169.99251	167.02516

Table S10 Selected bond lengths (Å) and bond angles (◦) for Ni(L^1) and Ni(L^2) at DFT-B3LYP level.

	Ni(L^1)	Ni(L^2)		Ni(L^1)	Ni(L^2)
Bond length	Å		Bond angles	◦	
N(1)-Ni(1)	1.85905	1.86021	C(17)-N(1)-Ni(1)	127.89581	127.90632
N(2)-Ni(1)	1.85991	1.86235	C(16)-N(1)-Ni(1)	112.12536	112.13069
O(1)-Ni(1)	1.85021	1.85542	C(10)-N(2)-Ni(1)	126.95844	126.97511
O(2)-Ni(1)	1.83548	1.83759	C(11)-N(2)-Ni(1)	113.98125	113.99326
C(3)-O(3)	1.43987	1.44025	O(2)-Ni(1)-O(1)	83.89169	83.90914
C(4)-O(3)	1.38011	1.38512	O(2)-Ni(1)-N(2)	178.54891	178.55012
C(8)-O(1)	1.31587	1.31932	O(1)-Ni(1)-N(2)	95.58654	95.59328
C(10)-N(2)	1.29015	1.29423	N(1)-Ni(1)-N(2)	87.28743	87.29542
C(11)-N(2)	1.48952	1.48992	C(17)-N(1)-Ni(1)	8.42361	8.48742
C(16)-N(1)	1.49825	1.49921	O(1)-Ni(1)-N(1)	178.58942	178.65812
C(17)-N(1)	1.29862	1.29898	O(2)-Ni(1)-N(2)	179.15847	179.16254
C(21)-O(4)	1.37625	1.37752	Torsion angles	◦	
C(23)-O(2)	1.31159	1.31524	C(16)-N(1)-Ni(1)-O(1)	158.95423	158.97252
C(24)-O(4)	1.42954	1.43026	C(16)-N(1)-Ni(1)-N(2)	13.05894	13.10254
C(23)-O(2)	1.31585	1.31745	C(11)-N(2)-Ni(1)-O(2)	174.19548	174.19852
C(8)-O(1)	1.31789	1.31932	C(10)-N(2)-Ni(1)-O(1)	11.21254	11.21845
			C(11)-N(2)-Ni(1)-N(1)	12.96521	12.97562

References

S1. (*a*) J. Marmur and P. Doty, *J. Mol. Biol.*, 1961, **3**, 585–594; (*b*) M. E. Reichmann, S. A. Rice, C. A. Thomas and P. Doty, *J. Am. Chem. Soc*., 1954, **76**, 3047–3053.

S2. J. Carmichael, W. G. DeGraff, A. F. Gazdar, J. D. Minna and J.B. Mitchell, *Cancer Res.*, 1987, **47**, 936–942.

S3. (*a*) C. R. Sihn, E. J. Suh, K. H. Lee, T. Y. Kim and S. H. Kim, *Cancer Lett.*, 2003, **201**, 203–210; (*b*) P. Heffeter, M. A. Jakupec, W. Korner, S. Wild, N. G. V. Keyserlingk, L. Elbling, H. Zorbas, A. Koryneuska, S. Knasmuller, H. Sutterluty, M. Micksche, B. K. Keppler and W. Berger, *Biochem. Pharmacol.*, 2006, **71**, 426–440.

S4. M. Ganeshpandian, R. Loganathan, E. Suresh, A. Riyasdeen, M.A. Akbarshad and M. Palaniandavar, *Dalton Trans.*, 2014, **43**, 1203–1219.

S5. K. P. Manas, M. S. Mobin, J. B. Ray and G. Prasenjit, *Inorg. Chim. Acta,* 2011, **372**, 145–151.

S6. P. Bhowmik, L. K. Das, S. Chattopadhyay and A. Ghosh, *Inorg. Chim. Acta*, 2015, **430**, 24–29.

S7. A. Guha, K. S. Banu, S. Das, T. Chattopadhyay, R. Sanyal, E. Zangrando and D. Das, *Polyhedron*, 2013, **52**, 669–678.

S8. P. K. Basu, M. Mitra, A. Ghosh, L. Thander, C. H. Lin and R. Ghosh, *J. Chem. Sci*., 2014, **126**, 1635–1640.